UNIVERSITA DEGLI STUDI DI TORINO

Department of Life and Health Sciences

PhD in Medical Pathophysiology

CICLO XXXVI

PhD Thesis

EXTRACELLULAR MATRIX AND TUMOR MICROENVIRONMENT: ROLE OF EXTRACELLULAR VESICLES

Tutor:
Benedetta Bussolati

PhD Candidate:
Dott.ssa Sarah Tassinari

2023

TABLE OF CONTENT:

ACKNOWLADGMENT:

I would like to thank Prof Benedetta Bussolati for the supervision, opportunities, and shared knowledge I have received during my stay in her laboratory.

I would like to thank my PhD supervisor for her daily support and presence, driving me, during these years, into personal and scientific growth.

I thank all the members of lab 10 in the Molecular Biotechnology Centre in Turin for all their guidance and sharing.

I would like to thank the Surgery and Gastroenterology Unit of the Molinette Hospital in Turin, especially the doctors Alessandro Musso, Giuseppe Giraudo, Marco Ettore Allaix, Giorgio Maria Saracco, Mario Morino for their patience and availability in the management of clinical protocol.

I also thank the Pathological Unit of the City of Science and Health of Turin, in particular Professor Paola Cassoni and Enrico Falco, for their help with surgical specimen processing.

I thank my students for helping me with this study, your support was precious. I would like to thank Roberta, with whom I shared this path from the beginning; Adele and Fabio for being fantastic and patient colleagues. Finally, I would like to thank all the people who I have met and collaborated with during these years. I would like to express my gratitude to everyone who has been a part of this work and part of my life.

I thank my family, that always supported me in every step of my life. The most special thanks to Enrico and Aurora, you bring the light.

NOTES

The study described in the present thesis is part of the following unpublished paper:

- Reconstructed colorectal cancer model to dissect the anti-tumor effect of mesenchymal stromal cells derived extracellular vesicles – D'Angelo E. et al. (Submitted, under revision)
- Profile of matrix-entrapped extracellular vesicles of microenvironmental and infiltrating cell origin in decellularized colorectal cancer and adjacent mucosa Tassinari S. et al. (Accepted)

ABSTRACT

Colorectal cancer (CRC) is the third most frequent and the fourth leading cause of cancer-associated mortalities worldwide. Tumor microenvironment (TME) is a complex entity composed of cellular and non-cellular elements. The invasion and growth of tumors and pre-metastatic tissues is heavily influenced by the presence of TME, which infiltrates and surrounds them.

- **EVs IN CRC MICROENVIRONMENT**
  The extracellular vesicles entrapped and stored within the extracellular matrix (ECM) may reflect the different populations enriched in the TME in different tumor stages generating a tissue microenvironment profile. To this aim, we isolated and characterized EVs from decellularized (CRC-ECM) and fresh surgical specimens of colorectal cancer (CRC-TISSUE), and adjacent normal colon mucosa (HC-ECM or HC-TISSUE) and analyzed their surface marker profile. The surface marker analysis showed different EV-related information from the different analyzed sources. Comparing EVs extracted from CRC-TISSUE vs HC-TISSUE we observed alteration of markers related to the cellular microenvironment and tumor phenotype. Analysis of EVs extracted from decellularized tissue showed a different markers distribution related to tumor stage. No difference in surface marker expression was observed between tumor and mucosa in low stage tumors. At variance, in the mucosa adjacent to high stage carcinomas, HC-ECM-EVs showed a significantly increased level of immune cell, epithelial and platelet markers in comparison with corresponding CRC-ECM-EVs as well as of low-stage tumors. In addition, ECM-EVs from high stage tumor specifically upregulated CD25, a T lymphocyte marker, observed to be increased also in CRC-TISSUE-EVs, possibly related to a regulatory phenotype. These results highlight the profile of EVs in colon carcinoma microenvironment and unprevail a profound change in the healthy mucosa adjacent to high grade tumors.

- **DECELLULARIZED ECM AS A 3D-CRC PATIENT DERIVED MODEL**
  The antitumoral activity of stem cell derived EVs has been intensively studied in different models. We here demonstrated that Mesenchymal Stromal Cell-derived EVs (MSC-EVs) injected in a three-dimensional (3D)-CRC model were able to mediate their therapeutic properties in patient-derived tumor decellularized matrices (TDM). Results on MSC-EVs treatment of HT29 in the repopulated TDM significantly reduced the invasion capabilities, impairing their proliferation as detected by the downregulation of the pro-proliferative genes (c-MYC, KI-67, CCND2, and CCNE1) and induction of apoptosis. Proteins upregulated (n=71) by the EV treatment in HT29-repopulated TDM, were mainly associated with chromatin silencing and glycolytic processes. On the contrary, the downregulated proteins (n=115) were primarily related to differentiation and ATP synthesis processes, with an over-representation of membrane and focal adhesion cellular components. It represents a promising biomarker to be further investigated for tumor diagnosis and progression. Finally, MSC-EVs were able to migrate inside tumor scaffolds and dynamically modify tumor cell-matrix interaction by activating selective anti-tumor programs.

In this study, we demonstrated that decellularized CRC tissue is an extracellular matrix model that permits to study EVs distribution in tumor microenvironment. Furthermore, this patient-derived 3D-CRC model is a useful tool for testing several types of therapeutics in colon cancer. We demonstrated that fresh biopsies contain EVs, exposing the heterogeneity of tumor and infiltrating cell composition (tumor cells, endothelial cells, platelets), their interactions and the resulting tumor state. At variance, EVs from decellularized tissues, entrapped in the extracellular matrix, may better embody the microenvironment alterations more prominent in the tumor surrounding tissue.

CHAPTER 1: INTRODUCTION

Extracellular Vesicles (EVs) are phospholipid bilayer covered particles derived from plasma membrane and released into the extracellular space by all cell types. MISEV guidelines define "extracellular vesicle" (EV) as the generic term for particles naturally released from the cell that are delimited by a lipid bilayer and cannot replicate, i.e., do not contain a functional nucleus. EVs are a heterogeneous population that can be manly subdivided according to dimension (small, medium, large vesicles), biochemical composition (CD63+/CD81+- EVs, Annexin A5-stained EVs, etc.) and cell of origin (podocyte EVs, hypoxic EVs, large oncosomes, apoptotic bodies).[1] Vesicles serve as a postal service for the information exchange between cells and the microenvironment modification.[2] In particular, EVs cargo molecules include a wide range of bioactive molecules such as proteins, lipids, DNA fragments, miRNAs, mRNAs and oncogenic virus-derived molecules exerting an autocrine, paracrine and endocrine signalling transduction. The surface of the extracellular vesicle is surrounded by protein (membrane protein and cargo protein) and nucleic acid. Membrane protein include tetraspanins (CD9, CD63, CD81, etc), adhesion molecules (integrins, EpCAM, Ephrin, etc.), MHC, and receptors. Nucleic acids include DNA and RNA (messenger RNAs (mRNAs), microRNAs (miRNAs), long non-coding RNAs (LncRNAs), and circular RNAs (circRNAs)).[3] EVs can be released into the extracellular environment under physiological or pathological conditions, such as inflammation, immune disorders, neurological diseases, and cancer. They can exert pleiotropic biological functions in target cells and can influence the microenvironment via the release of bioactive molecules.[4]

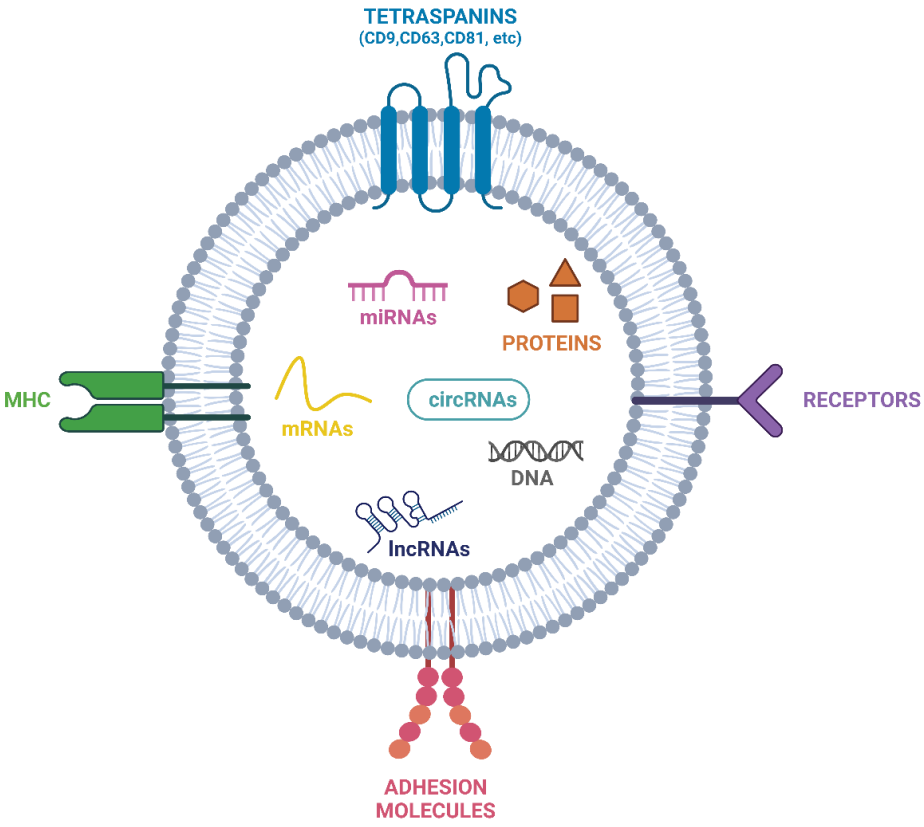

Figure 1 *– Schematic representation of EVs Composition and structure*

1.1 COLORECTAL CANCER

Colorectal cancer (CRC) is the second leading cause of cancer death and is the third most diagnosed cancer worldwide. Many risk factors have been associated with CRC, such as smoking, an unbalanced diet (including high consumption of red meat and low consumption of fruits and vegetables), high alcohol intake, obesity, physical inactivity, and sedentary lifestyle[5]. In 2020, more than 1.9 million CRC new cases have been estimated and about 1 million deaths have occurred worldwide, representing the 10.7% and 9.5% respectively of all new cancer cases and deaths. It has been 60,4% of all CRC cases were aged between 50 and 74 years at diagnosis, while the cases diagnosed under 50 years represent about 10% of total diagnosis. Half of all CRC death occurred between 50-74 years old group. It has been hypothesized that by 2040, diagnosed CRC cases will rise to 3.2 cases if the incidence rate remains unchanged. It is a 63% increase over 2020 when 2 million cases were estimated. Deaths are also expected to increase by 73.4%, from 0.9 million deaths in 2020 to over 1.6 million deaths in 2040. [6] CRC carcinogenesis is characterized by several phases (Fig.3):

- Initiation: it involves irreversible genetic alterations that predispose the affected cells to neoplastic transformation.
- Promotion: the initiated cells start to proliferate with abnormal growth mechanisms (neoplasm).
- Progression: the cells undergo further genetic and epigenetic mutations that could confer a selective growth advantage, inducing also benign tumor cells to switch into malignant cancer cells and acquire aggressive characteristics and metastatic potential.
- Metastasizing: cancer cells from primary organ spreads to other organs or tissues through the bloodstream or the lymphatic system[7].

About 60-65% of CRC cases develop sporadically due to acquired genetic and epigenetic aberrations caused by potentially modifiable risk factors. About 25% of CRC cases occur in people with a family history of the disease, but without any known genetic cancer syndrome. Only 5% are caused by hereditary cancer syndromes such as Lynch syndrome or familial adenomatous polyposis, which are caused by inherited genetic mutations in high-penetrance susceptibility genes. [8]

CRC development can follow three distinctive pathways (Fig.3):

a. Adenoma–carcinoma sequence: this pathway is present in the majority of sporadic CRC. Normal cells progress to small adenoma, to large adenoma and, finally, to cancer.
b. Serrated pathway: progression from normal cells to hyperplastic polyp, to sessile serrated adenomas and, finally, to cancer.
c. Inflammatory pathway: driven by chronic inflammation, normal cells progress to indefinite dysplasia, to low-grade dysplasia, to high-grade dysplasia and, finally, to cancer.[5]

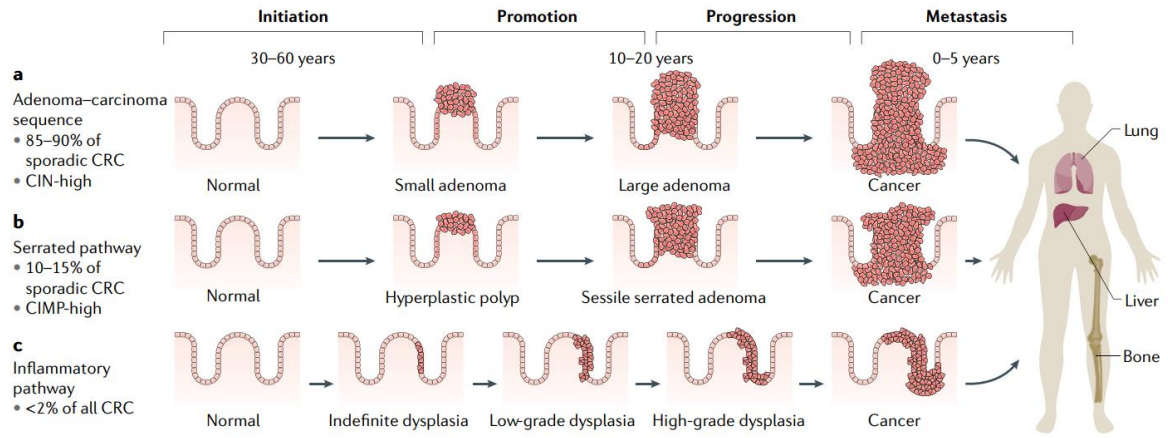

Figure 2 - *CRC carcinogenesis mechanisms*[5].

The World Health Organization (WHO) has defined different subtypes of colorectal cancer (CRC) based on their histopathologic appearance[9]:

- Adenocarcinoma with formation of glandular structures and without excessive mucus production.
- Mucinous carcinoma if mucus production is observed in over 50% of the tumour mass. Is predominantly located in the right colon.
- Medullary carcinomas are poorly differentiated and characterized by the presence of solid sheets or nests of malignant cells with pushing borders, prominent intraepithelial lymphocytic infiltration, and little to no gland formation. Like mucinous carcinomas, medullary carcinomas are more common in the right colon.
- Signet ring cell carcinoma is another rare histologic subtype that accounts for less than 1% of colorectal carcinomas and is characterized by the proliferation of cells with intracellular mucin pools that displace the nucleus to the side. This type of tumour is often diagnosed in younger patients, and up to 40% of cases have been observed to be associated with the right colon.

Determining the stage of colorectal cancer (CRC) through clinical and pathological assessments is crucial for predicting the prognosis and developing a treatment plan. This staging process helps determine the extent of the cancer, both locally and in other parts of the body. The AJCC-UICC tumour node metastasis (TNM) staging system, which was last updated in 2017, is the widely accepted and considered the gold standard for prognosticating newly diagnosed CRC patients.[10] The T component of the TNM staging system for colorectal cancer (CRC) is determined by the extent of local tumour invasion into various layers, including submucosa (Tis or T1), muscularis propria (T2), adventitia (T3), visceral peritoneum (T4a, but only if intraperitoneal), or beyond into other structures (T4b). The N stage reflects the number of positive regional lymph nodes. M staging specifies the number of other solid organs involved, up to 2 (M2). CRCs stages are divided into prognostic stage groups from I to IV, with subgroups indicated by letters to signify a progressively worse prognosis. Stage I and stages IIA to IIC CRC are classified as N0, while stage IV is classified as M1 or M2. Stages IIIA to IIIC are composed of different combinations of T and N stages (table 1).[11]

Table 1 - *prognostic group of CRCs staging based on TNM classification system.* [9]

Stage	Definition
0	Carcinoma in situ: invasion confined to the mucosal lamina propria (Tis)
1	Invasion of the submucosa (T1) or muscularis propria (T2)
2A	Invasion through the muscularis propria (T3)
2B	Invasion of the visceral peritoneum (T4a)
2C	Invasion of other organs or structures (T4b)
3A	– T1 or T2 tumor with the presence of metastasis in 1–3 regional lymph nodes (N1) – T1 tumor with the presence of metastasis in 4–6 regional lymph nodes (N2a)
3B	– T1 or T2 tumor with the presence of metastasis in 7 or more regional lymph nodes (N2b) – T2 or T3 tumor with the presence of N2a metastasis – T3 or T4a tumor with the presence of N1 metastasis
3C	– T3 or T4a tumor with the presence of N2b metastasis – T4a tumor with the presence of N2a metastasis – T4b tumor with the presence of N1 or N2 metastasis
4A	Presence of metastasis confined to one organ without peritoneal metastases
4B	Presence of metastasis in more than one organ
4C	Presence of metastasis to the peritoneum with or without other organ involvement

CRC is a complex and heterogeneous disease and, as previously described, has a high incidence in the world population. Despite initial treatment with surgery and chemotherapy and advances in therapies (such as immune checkpoint inhibitors), CRC recurrence and metastasis remain the leading causes of death. [12] Being able to have an early diagnosis is a key step in acting early and avoiding recurrence. Today there are already biomarkers such as CEA, which is the main tumour marker used for suspected gastrointestinal tract cancers, but it is not typically elevated in the early stages of the disease. [13] Therefore, more clinical biomarker resources are needed.

1.2 THE TUMOR MICROENVIRONMENT:

in cancer development and progression.[14] The tumor microenvironment (TME) is a complex entity composed of cellular and non-cellular elements that surround the tumor and promote its growth. TME can also influence the permeation, distribution, and metabolism of therapeutic agents as well as produce molecular factors and signals which positively or negatively regulate how the tumor cells respond to therapy.[4] In detail, TME consists of different stromal components that are co-evolved with cancer cells and contribute to cancer progression and metastasis such as fibroblast, immune cells, and endothelial cells.[15–17] The communication between cancerous cells and the tumour microenvironment (TME) is facilitated by cancer-associated fibroblasts (CAFs), which are a crucial constituent of the tumour stroma. A frequent link between the accumulation of CAFs within the TME and an unfavourable prognosis in various types of cancer has been observed. For example, in colorectal cancer, the presence of CAFs is highly correlated with a higher likelihood of disease recurrence.[18] Endothelial cells are key player in promoting cancer cell migration, and cancer cell protection from the immune system.[19] As the tumour undergoes growth, it exhibits an increased demand for oxygen and nutrients, thereby inducing angiogenesis - a biological process that results in the formation of blood vessels, which typically emerge from existing vessels or derived by endothelial

progenitor. Stromal cells provide oxygen and nutrients via the vasculature as well as soluble and matrix-bound growth factors and enzymes that exert significant influence on the processes of angiogenesis, proliferation, invasion, and metastasis[18,20]. Immune cells, which include granulocytes, lymphocytes, and macrophages, are the second major component and are involved in a variety of immune responses. The non-cellular TME component, together with EVs, is composed also of extracellular matrix (ECM) that represents the most abundant component, and of secreted metabolites acting as players in TME communication. ECM is a collection of structural components (collagen, laminin, fibronectin, glycans, proteoglycans, and hyaluronic acid) and non-structural secreted enzyme (growth factors, hormones, and remodeling protease) that play a crucial role in tumor progression and diffusion. Initially considered as an amorphous scaffold in which cells are organized, in the past years, ECM has been proposed as a crucial player in tumor progression and diffusion. Solid tumors contain large ECM deposits and constitute up to 60% of tumor mass. Proteases release cytokines and growth factors, which are stored in the ECM.[18,21]

1.3 EVs IN CANCER AND IN TME

The first evidence that tumor cells shed membrane vesicles was provided in 1978 from Friend and colleagues but only in the first decade of the 21st century, it was formally proven that EVs are not artifacts and can affect tumor progression by promoting different mechanisms.[22] Today we know that cancer cells communicate using EVs, by transferring information at paracrine level. Several reports showed that EV cargo influences the stroma by activating a molecular pathway that differs, in part, from the ones modulated by soluble factors.[23] Tumor pathogenesis is characterized by multiple steps such as the occurrence of genetic mutations, evading and corruption of the immune system, following by modifications of the surrounding microenvironment. Although a lot of genome alterations have been identified in cancer, less is known about the role of cell and tissue microenvironment interactions Through EVs, all these cells and components interact with each other and are a factor in TME diversity (Fig.2).[24] In fact, cells release EVs to communicate in long-distance, which requires EVs to traverse the ECM. Although the transport mechanism of EVs through the ECM has not been clarified yet, it was recently observed that, in contrast to synthetic nanoparticles, EVs are easily transported through nano porous ECM. [25] EVs are also be detected in ECM bio-scaffolds produced by the decellularization of source tissues and the signature of extracellular vesicles detected in ECM (ECM-EVs) was distinctively different between the different source tissues from which the bioscaffolds were prepared.[26] It has been demonstrated that tumor cells take advantage of EVs functions via transformation from a normal microenvironment into a TME. Vesicles that normally support and protect normal tissues, start to support the growth of tumor tissue providing nutrient and helping tumor cells to escape the immune system.[27] However, available data suggest that EVs can also retain anticancer properties and may act to suppress disease progression. Although, EVs function has been investigated in several types of cancer over the past two decades in several studies, their precise role remains uncertain. [28] Furthermore, in tumor pharmacological treatment, changes in TME are often an obstacle. The success of anticancer therapy is usually limited by the development of drug resistance. Such acquired

resistance is driven, in part, by heterogeneity, the phenotypic diversity of cancer cells within a single tumor mass.

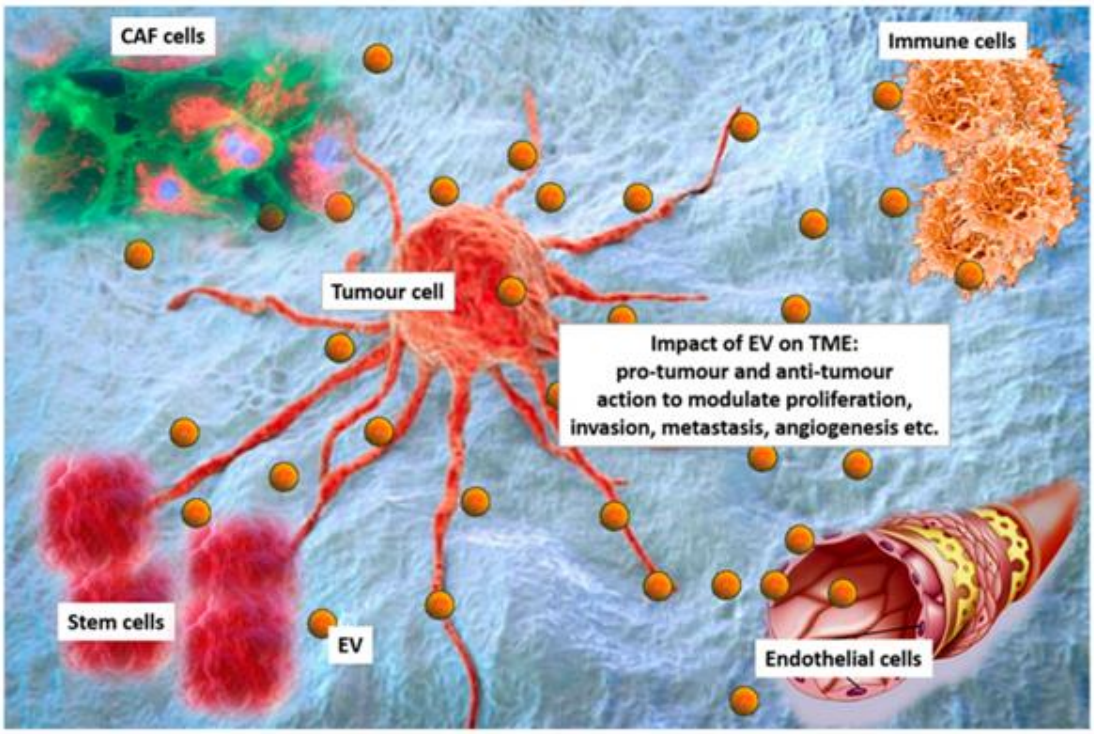

Figure 3 - EVs in the Tumor Microenvironment [24]

Since EVs cargo contains information on cell sub-proteome, it can either be used as a source of disease biomarkers or drug delivery vehicles. Moreover, EVs contain cancer patient-specific genes which can be used for cancer diagnosis. Besides serving as a source of biomarkers, EVs also have potential to be used as drug delivery systems, allowing personalized chemotherapy. Compared with other nanocarriers, EVs, are made of natural lipid bilayers that adhere to their protein cargos that in turn interact with cellular membranes. Also, since EVs can derive from the same patient, they are less toxic and are less immunogenic than any foreign delivery vehicle, drastically improving the drug therapeutic efficacy.

1.4 MESENCHYMAL STEM CELLS DERIVED EVs IN TUMOR

Mesenchymal stem cells (MSCs) are non-hematopoietic cells that can undergo self-rejuvenation and differentiation into different cell types such as muscle cells, hepatocytes, osteoblasts, adipocytes, chondrocytes, and stromal cells[29]. Due to their unique properties, such as low immunogenicity and powerful immunomodulatory and immunosuppressive capabilities, they have become ideal candidates for cell-based therapies[30]. MSCs are important cellular component of the TME and interact with cancer and other cells in the TME via paracrine factors and through extracellular vesicles (EVs) to support tumour growth, progression, and metastasis[31]. However, the exact mechanism by which MSCs influence cancer remains controversial playing a dual role in tumorigenesis and cancer progression[32]. On one hand, they promote the anchoring of cancer cells in the tumour stroma and support cancer

development[33]. In particular, they generate a tumour-friendly microenvironment through the release of pro-tumorigenic factors[34], the support of angiogenesis mechanisms, the initiation of epithelial–mesenchymal transition (EMT), the differentiation into CAFs[35], and the disruption of the immune surveillance[36–38]. On the other hand, many studies revealed that MSCs could suppress tumour development by inhibiting angiogenesis process and improving the infiltration of inflammatory cell, apoptosis, and cell cycle arrest, together with the reduction of AKT and Wnt signalling pathways[37]. Furthermore, current studies suggests that paracrine mechanisms, such as the secretion of a wide array of growth factors, cytokines, and extracellular vesicles (EVs), are responsible for the therapeutic effects of MSCs[39,40]. MSC-derived extracellular vesicles (MSC-EVs) are vectors in the communication between MSCs and TME[41]. It has been shown that MSC-EVs are mimicking all the properties of maternal cells, especially the paracrine effects and immunomodulatory functions. Pre-clinical data and clinical trials demonstrated the safety and scalability of MSC-EV production for clinical applications. Additionally, MSC-EVs exhibit outstanding biocompatibility and exceptional biodistribution abilities, which include the capacity to overcome biological barriers, low toxicity and immunogenicity, and powerful tumour tropism[42]. Moreover, engineered MSC-EVs have been used as a promising strategy for the treatment of different diseases, including cancer[43]. In fact, bioengineered MSC-EVs can be moulded with therapeutics like miRNAs, proteins, or chemotherapeutic drugs to improve cancer targeting precision, efficiency, and safety[42]. What is more, different MSC-derived EVs (MSC-EVs) have been implicated in matrix remodelling during wound healing processes and fibrogenesis, supporting their capability to alter ECM composition in pathophysiology [44,45]. The TME complexity makes the use of MSC-EVs for cancer treatment more challenging, compared to regenerative medicine. MSC-EVs' therapeutic application is still in development, and there is often uncertainty about their precise functional mechanism of action. To maximize the hidden potential of MSC-EVs, further research is required.

1.5 3D MODEL IN CANCER BIOLOGY

Cancer research has been based on in vitro 2D cell cultures, in vivo xenografts, or genetically engineered animal models for many years. However, these conventional models are unable to sustain the complexity of tumor samples from human patients as well as to mimic the disease pathogenesis, allowing easy cellular and environmental manipulation[46]. The use of 2D immortalized cell lines has been widespread because of their accessibility, reproducibility, high throughput, and low cost. In particular, they have been used extensively as an initial screening model to unravel the mechanisms of cancer biology and for drug screening[47,48]. Nevertheless, these systems have several disadvantages:

- The isolation and growth of cancer cell lines derived from patient biopsies can be challenging.
- Patient-derived cells are growing into a flat synthetic surface that doesn’t mirror the tissue morphology changing the TME or the response to specific stimuli[49–51].
- Clonal selection is usually used to select cells in 2D models, producing a cell line that does not preserve the genetic heterogeneity of the parental tumor[52].

- The effectiveness of cancer therapy is negatively impacted by the insufficient pairing of in vitro cancer cell lines with patient-matched 2D normal tissue and lack of information on the 3D TME interaction of the patient's tumor[53,54].

2D co-culture system has been created to partially simulate the complexity of in-vivo cell to cell communication. Cancer cell lines have been combined with different types of exogenous cells (CAFs or Peripheral Blood Mononuclear Cells, PBMCs)[55]. Anyway, this 2D reconstructed system failed to fully model the 3D structure and complexity of TME. Preclinical in vivo animal models provide models that consider the 3D tumor tissue organization, which allows the analysis of tumor onset, progression, and drug response[56,57]. More in detail, these models include patient-derived xenografts (PDXs) and genetically engineered mouse models (GEMMs). PDXs are made by transferring subcutaneously or orthotopically freshly derived patient material into immunodeficient mice and allow easy tumor growth and precise monitoring of tumor progression[58–61]. However, PDX models present a lack of adaptive immune response and the progressive replacement of human cell with recipient mouse cells that constitutes an inappropriate response prediction for screening and functional assay of therapeutic agents[62,63]. On the contrary, GEMMs develop tumors in an immunoproficient animal enabling the genesis of a model with native interactions between cancer cells and TME useful for immunotherapies screening[64]. Anyway, there are still some aspects that need to be improved. In example, the process of introducing novel (non-germline) mutations is laborious and slow due to their relatively limited genetic manipulation[56]. On the whole, PDX and GEMM are expensive, time- and resource-consuming, relatively low-throughput models. Furthermore, there is a growing ethical pressure to find alternative solutions that comply with the 3Rs principle in animal experimentation[65]. To fill this gap, researchers developed more sophisticated in vitro 3D systems which can recreate human organs and diseases. In fact, recently the attention in cancer research has been increasing towards 3D cell models that replicate several hallmarks of in vivo tumors. The architecture of the tissue in these systems is more realistic compared to 2D cell cultures and provides a multicellular complexity that allows for dynamic interaction between cancer cells and TME[66,67]. One of the most established 3D culture methods can be spheroids: micro-sized aggregates of compacted cells which recreate many solid tumors characteristics including tissue structure. cellular heterogeneity, signaling pathways and interactions between cells and ECM, growth, gene expression and drug resistance[68,69]. For these characteristics, spheroids can be used as suitable in vitro tools for high-throughput screening of anticancer therapeutics[70]. Despite this, the absence of standard protocols and methods to establish spheroids of uniform size and shape remains a major challenge in using them as preclinical cancer models. Furthermore, certain methods are linked to low throughput and trouble in acquiring cells for readout analysis[71]. Additionally, spheroids fail to represent the complexities found in the 3D tissue architecture of living organs because they do not include mechanical forces that can significantly affect the behavior of cancer cells.[72] Another strategy to obtain 3D in vitro tumor model is represented by organoids. These stem cell derived 3D cultures are used to replicate the cellular multiplicity, tissue organization and purpose. Moreover, organoids are capable of self-organization and self-renewal[73–75]. Organoids have been a great tool for studying the mechanism of cancer initiation and progression in different organs in different organs as well as the tumor niche formation factors requirements[76,77]. Moreover, they have been used to evaluate the cellular response to anticancer therapies connected to mutation pathways. Furthermore, patients-derived organoids can be easily propagated from a small sample of solid/liquid biopsies or surgical specimens of primary

tumors[78], circulating cancer cells[79] and metastasis[80]. Unfortunately, creating organoids derived from patients, which are useful tools for studying phenotypic and genetic resemblances and personalized cancer therapy, is unfortunately just a proof-of-concept[78,80]. Organoids can also be utilized to better understand and predict treatment-related side effects, which are frequently observed in targeted therapy. Despite their various advantages, the application of tumor organoids in a clinical setting may be hindered by the inability to obtain stromal components and an immune-competent microenvironment[81]. Hence, the improvement and integration of 3D cancer models, such as cancer spheroids and organoids, help to recreate the complexity of the TME to evaluate the roles and interactions of individual cellular and non-cellular players in tumor progression and therapy response[82]. The refinement of these 3D cancer models and the development of new ones should be one of the most important goals in the cancer field to reduce and replace animal studies, while helping human patients.

1.6 STATE OF THE ART AND AIM OF THE STUDY

Several studies have shown that extracellular vesicles (EVs) obtained from cancer patients are related to disease status and can be detected even in the early stages of cancer.[83,84] It has been reported that EVs carry a variety of molecules, such as proteins, lipids, and nucleic acids, which can have a profound effect on recipient cells and reflect the phenotype of their parental cells.[85,86] Therefore, extracellular vesicles in the tumour microenvironment can provide information about the progress or alteration of cancer cells. These observations lead to the inference that EVs represent an important mediator of intercellular communication within the tumour microenvironment, with implications for the development of new therapeutic and diagnostic strategies. The role of EVs in the tumour microenvironment has been studied in several types of tumour models, showing that EVs can mediate migration, invasion, angiogenesis, and survival of cancer cells.[87] Specifically, stress conditions such as hypoxia, starvation, and acidosis act as positive feedback for tumours by increasing EVs release from cancer cells, resulting in changes and expansion of the TME. [88–90] Tumour-derived sEVs can contribute to the epithelial-mesenchymal transition (EMT) process, characterized by a loss of epithelial properties, and gain of mesenchymal properties. EMT is considered one of the most crucial mechanisms required for tumour metastasis. In addition, cancer derived EVs may impair immune cell maturation and antitumor activity, establishing an immunosuppressive microenvironment and promoting the immune escape of cancer cells.[91] Therefore, the role of extracellular vesicles in the development and progression of CRC is central because of their participation in bidirectional signalling between cancer cells and TMEs at each stage of CRC carcinogenesis. Their detection in a wide variety of biological fluids represents the future of cancer diagnosis. Moreover, due to their minimally invasive sampling method and convenient accessibility, EVs are suitable for sequential collection. Therefore, EVs have great potential as useful biomarkers that can provide information on disease conditions in a minimally invasive manner. Most of the EVs studies have employed in vitro cell lines or body fluids as sources of EVs, whereas the number of research studies conducted on EVs derived from tissue is still limited. The first protocol for extraction of extracellular vesicles isolated from colorectal tissue was published in 2021 by Crescitelli et al. [87] and was adopted in this study. This project aims to identify the role of EVs from tumor microenvironment, in the CRC. The purpose of our

study was therefore to better understand the pathological mechanisms involved in CRC progression involving the interaction between EVs and TME and to identify a possible CRC signature possibly useful as biomarkers of diagnosis and staging. As EV surface markers reflect the originating cells, the characterization of EVs within ECM could elucidate the composition of the tumor microenvironment and its changes during tumor progression. We therefore reasoned that the analysis of the different EV subpopulations within TME and surrounding non-infiltrated mucosa may provide a signature of the different populations representing the tumor microenvironment and of their possible interactions. We isolated and characterized EVs from 23 colorectal cancer decellularized surgical specimens (CRC-ECM-EVs) and 104 fresh CRC surgical specimens (CRC-EVs), and analyzed the surface profile composition, in comparison with that of normal colon decellularized or fresh mucosa (HC-ECM-EVs or HC-EVs) from the same patient. Furthermore, to highlight the capability of EVs to diffuse into tumour ECM and be up taken from engrafted colon cancer cells, we used decellularized tissues as three-dimensional (3D) colorectal cancer model. Moreover, we questioned whether and how, MSC EVs (MSC-EVs) might influence colorectal cancer cells engraftment and proliferation as well as affect the structural components of the ECM. In fact, we propose that the selective EVs tropism for tumour and non-tumour components can be used as an anti-tumour drug delivery platform.

CHAPTER 2: MATERIALS AND METHODS:

2.1 PATIENTS AND CONSENT:

This study was conducted according to the principles expressed in the Declaration of Helsinki. Written informed consent was obtained from every enrolled individual, and the protocol was approved by the ethics committee of institutional (Ethical Committee Approved Protocol Number: 448/2002). All the patients enrolled fulfilled the following inclusion criteria: histologically confirmed primary adenocarcinoma of the colon, age of more than 18 years, and written informed consent. Patients with a known history of a hereditary colorectal cancer syndrome and patients that underwent neoadjuvant treatments were excluded. CRC tissues were obtained at the edge of infiltrating neoplasia while healthy colon mucosa was obtained >10 cm far from the cancerous lesion.

2.1.1 DECELLULARIZED TISSUE:

ECM model for EVs extraction and 3D model has been obtained by the decellularization of human colorectal cancer biopsy and normal colon biopsy as a control. Decellularization procedure was conducted as previously described[14] starting from tissue samples from CRC patients who underwent curative surgery between February 2015 and December 2021 were collected from Tissue biobank of the General Surgery 3 (University-Hospital of Padova). A total of 23 primary colon tumour biopsies (CRC-ECM) and the corresponding normal colon mucosa (HC-ECM) were processed to isolate EVs for different analyses (Table 2). A series of 9 pathologic tissue samples from CRC patients has been used to recreate the 3D ECM model (Table 3).

2.1.2 FRESH BIOPSY:

A total of 104 fresh CRC surgical specimens (CRC-TISSUE) and coupled normal (HC-TISSUE), 11 fresh biopsy specimens (CRC-TISSUE), 8 fresh diverticulitis surgical specimens as a positive inflammatory control (normal (HC-TISSUE) were processed to isolate EVs for different analyses.

Table 2 - Clinical-pathological characteristics of decellularized study CRC patients enrolled for ECM-EVs extraction. T: Tumor; N: Node; M: Metastasis; TNM: Tumor Node Metastasis stage; G: Grade: TNM was defined according to the AJCC/UICC TNM staging system (8th ed.).

Patient	Sex	Age	T	N	M	TNM	G
01	M	82	4a	1b	1b	4b	2
02	F	76	3	1b	1a	4a	2/3
03	M	69	3	2b	1a	4a	2/3
04	M	74	3	2a	1c	4a	3
05	M	54	4a	2b	0	4a	3
06	M	81	4a	1a	0	3b	2
07	F	84	3	0	0	2a	1
08	F	75	3	0	0	2a	3
09	F	75	3	0	0	2a	2
10	F	85	3	0	0	2a	2
11	F	76	3	0	0	2a	1/2
12	M	82	3	0	0	2a	2
13	M	59	4b	0	0	2b	2
14	M	47	3	2a	1c	4c	3
15	M	79	4a	2b	1a	4a	3
16	F	55	3	2a	1a	4a	3
17	M	63	4a	1a	1c	4c	3
18	F	77	3	2a	1a	4a	2/3
19	M	80	3	1b	1a	4a	2
20	F	80	3	2a	1a	4a	3
21	F	63	4a	1b	1a	4a	3
22	F	52	3	1b	1c	4c	3
23	F	83	3	0	1a	4a	2/3

Table 3 - Clinical-pathological characteristics of decellularized study CRC patients enrolled for 3D patient derived ECM model. Data are expressed as number of patients. TNM: Tumor Node Metastasis stage; (%) unless stated otherwise. TNM was defined according to the AJCC/UICC TNM staging system (8th ed.).

		Patients (9)
Age	Median (range), yrs	65 (39-91)
Sex	Male (%)	4 (44)
	Female (%)	5 (56)
TNM	2 (%)	5 (56)
	3 (%)	4 (44)
Grade	1 (%)	1 (11)
	2 (%)	7 (78)
	3 (%)	1 (11)

2.2CELL CULTURE

Human colon epithelial cancer cells (Caco-2) were cultured in Dulbecco's Modified Eagle Medium (DMEM) medium (Gibco, Thermo Fisher Scientific, MA, USA) with non-essential amino acids (Gibco), 10% foetal calf serum and 1 mM glutamine, 10 mg/mL penicillin, and 10 mg/mL streptomycin and were kept at 70–80% confluency. HT29 were grown in Roswell Park Memorial Institute (RPMI) 1640 Medium (EuroClone, Milan, Italy) supplemented with 10% foetal bovine serum (FBS) (HyClone, Pittsburgh, USA), 1 mM glutamine, 10 mg/mL penicillin, and 10 mg/mL streptomycin. A lentiviral produced HT29 cell line carried both the ZsGreen fluorescent protein and the firefly luciferase under the EF1-alpha promoter was used for tracking analysis and was a gift from Dr. Luca Urbani (Institute of Hepatology, Foundation for Liver Research, London, UK). MSCs were obtained from Lonza (Lonza, Basel, Switzerland) and cultured in MSC basal medium (MSCBM, Lonza). MSCs were used up to the sixth passage of culture.[92] All cell cultures were maintained at 37◦C in a 5% CO2 humidified atmosphere.

2.3ISOLATION OF EVS

2.3.1 ECM-EVs:

The decellularized matrix underwent enzymatic digestion to allow the detachment of the EVs. Collagenase and Proteinase K (both 1 mg/ml in RPMI), affecting different membrane components were tested. The Proteinase K treatment showed the best results as number of EV recovered/integrity. Briefly, decellularized tissues were weighed, cut into small pieces and then digested for 40 min at 37°C under constant shaking. After incubation, the digested pieces were kept on ice to inactivate the enzyme and then transferred into a 40μm pore size (BD Falcon, NJ, USA) cell strainer and washed with 5ml PBS to permit EV release. The filtered solution was subjected to differential centrifugation and the supernatant was finally ultracentrifuged at 100,000 x g (Beckman Coulter Optima L-90K ultracentrifuge; Beckman Coulter, CA, USA) for 2 h at 4°C using a type 70ti rotor. Collected EVs were then resuspended in serum-free RPMI-1640 supplemented with 1% DMSO. The isolation process is summarized in Fig.4.

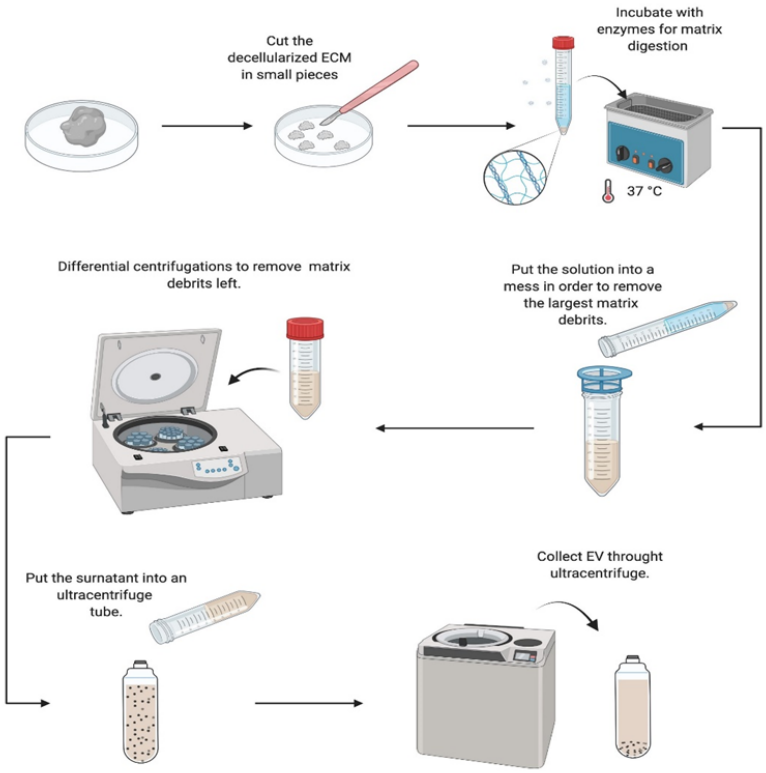

Figure 4 - schematic protocol of EVs isolation from decellularized tissues Directly from accepted paper: Profile of matrix-entrapped extracellular vesicles of microenvironmental and infiltrating cell origin in decellularized colorectal cancer and adjacent mucosa – Tassinari S. Et al.

2.3.2 TISSUE-EVs:

Tissue-EVs extraction protocol was adapted from the one described by Crescitelli et Al.[87] The tissue was maintained in MACS Tissue storage solution before being immediately processed for EV isolation. To standardize the EVs isolation protocol, EVs were obtained from 0.2g tissue. The tissue was first rinsed with sterile PBS. Afterwards, it was carefully cut into small piece (2 x 2 x 2 mm), and placed in a six-well plate in which a combination of enzymes were added; collagenase D (2mg/ml), DNase I (40 U/mL) plus 2ml of RPMI-1640, specifically prepared for biopsies (2,5 µg/ml Amphotericin B, 50 µg/ml Gentamycin,) in order to cover the entire tissue and allowed the enzymes to act on their entire surface. Then the plate was incubated for 30 min at 37 °C under mild agitation, and subsequently placed at 4°C to inactivate the enzymes. The solution and the digested pieces were then transferred into a cell strainer with 40µm pore size (BD Falcon, NJ, USA) and let the liquid drain through by gravity. The filtered solution was centrifuged, to remove debris, at 300 x g for 15min at 4°C and after transferring the supernatant into a new tube, centrifuged at 2000 x g for 20min at 4°C. The supernatant was ultracentrifuged at 100000g for 2 hours at 4°C using a 70ti rotor. EVs were then resuspended in RPMI with 1% DMSO. The isolation process is summarized in Fig.5.

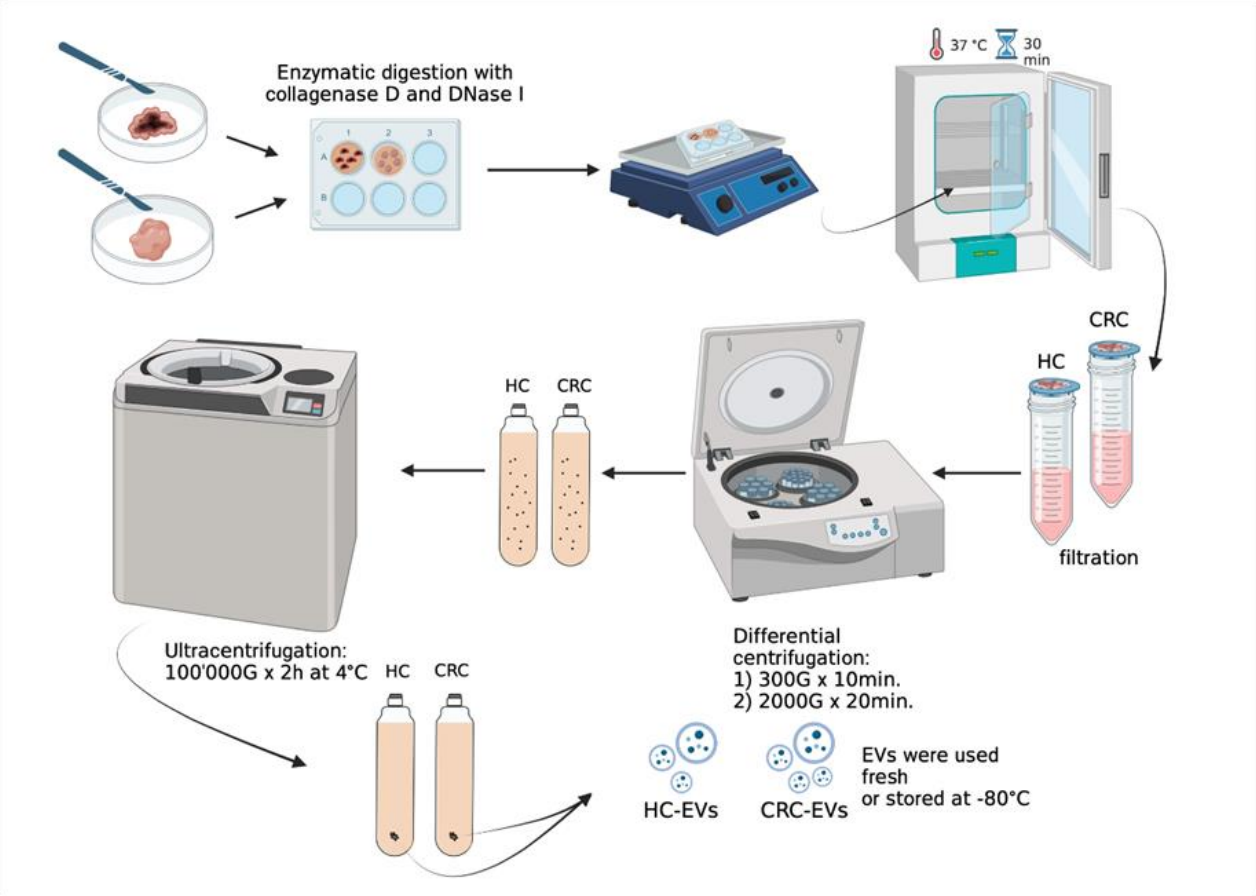

Figure 5 - schematic protocol of EVs isolation from fresh tissues.

2.3.3 MSC-EVs:

EVs were collected from MSCs after overnight starvation with serum-free RPMI-1640 (Lonza). The cell supernatant was collected and centrifuged for two times at 3,000 x g for 20 minutes to remove possible cell debris or apoptotic bodies. Then the supernatant was ultracentrifuged at 100,000 x g for 2 hours at 4°C using a 70ti rotor (Beckman Coulter Optima L-90K ultracentrifuge; Beckman Coulter, Brea, CA, USA). EVs were then resuspended in serum-free RPMI-1640 supplemented with 1% DMSO and stored at -80°C.

2.4 CHARACTERIZATION OF EVS AND TISSUES:

2.4.1 TEM:

Transmission electron microscopy (TEM) was performed to characterize the structure of vesicles; it was carried out using one drop of EVs solution (about 25µl) placed on 400 mesh holey film grid. After staining with 2% uranyl acetate (for 2 minutes) the sample was observed with a Tecnai G2 (FEI) transmission electron microscope operating at 100 kV. Images were captured with a Veleta (Olympus Soft Imaging System) digital camera. TEM was conducted also to investigate the presence of vesicles trapped inside the decellularized or un-decellularized tissue. Full tissues were fixed with 2.5% glutaraldehyde in 0.1M sodium cacodylate buffer pH 7.4 overnight at 4°C. The samples were postfixed with 1% osmium

tetroxide in 0.1M sodium cacodylate buffer for 1 hour at 4°C. After three water washes, samples were dehydrated in a graded ethanol series and embedded in an epoxy resin (Sigma-Aldrich). Ultrathin sections (60-70 nm) were obtained with an Ultrotome V (LKB) ultramicrotome, counterstained with uranyl acetate and lead citrate and viewed with a Tecnai G 2 (FEI) transmission electron microscope operating at 100 kV. Matrices were fixed with 2 % glutaraldehyde in 0.1 M phosphate; following washing they were cut into segments of approximately 1 cm length and cryoprotected in 25 % sucrose, 10 % glycerol in 0.05 MPBS (pH 7.4) for 2 h, then fast frozen. At the time of analysis, samples were processed as previously described[14]. Images were recorded with a Jeol 7401 FEG scanning electron microscope.

2.4.2 NANOPARTICLES TRACKER ANALYSES (NTA):

Concentration and size distribution of EV were determined by Nanoparticle tracking analysis (NTA) using the Nanosight LS300 system (Malvern Panalytical, Malvern, UK) equipped with a 488 nm laser module. Briefly, EVs were diluted (1:100) in sterile saline solution and analysed using the NTA 3.2 Analytical Software. Three videos of 60 seconds at camera level 14 and threshold 3 were captured using a syringe pump 30. The NTA settings were kept constant between samples.

2.4.3 SUPER-RESOLUTION MICROSCOPY:

Single ECM-EV surface marker analysis was conducted using a temperature-controlled Nanoimager S Mark II microscope from ONI (Oxford Nanoimaging, Oxford, UK) equipped with a 100x, 1.4NA oil immersion objective, an XYZ closed-loop piezo 736 stage, and 405 nm/150 mW, 473 nm/1 W, 560 nm/1 W, 640 nm/1 W lasers, as described [9]. EV profiler Kit (ONI) was utilized for the experiments following manufacturer's protocol. The Kit contains fluorescent antibodies anti CD9-488, CD63-568 and CD81-647. dSTORM mode acquired sequentially in total reflection fluorescence (TIRF) mode was used for the acquisition of images (2000 frames for each channel). Before each imaging session, beads slide calibration was performed to align fluorescent channels, achieving a channel mapping precision smaller than 12 nm. Single-molecule data was filtered using NimOS software (v.1.18.3, ONI). Data has been processed with the Collaborative Discovery (CODI) online analysis platform (www.alto.codi.bio) from ONI and the drift correction pipeline version 0.2.3 was used.

2.4.4 CYTOFLUORIMETRIC BEAD-BASED ANALYSES

EV surface markers were investigated using a bead-based cytofluorimetric analyses using the human MACSPlex exosome kit (Miltenyi Biotec, Bergisch Gladbach, Germany). Shortly, $1*10^9$ EVs were diluted with MACSPlex Buffer to a final volume of 120 µL. A total of 15 µL of MACSPlex exosome capture beads (FITC-PE), which contain beads coupled to 37 exosomal surface epitopes and 2 control isotypes, were added to the ECM-EVs that were incubated overnight at 4°C on an orbital shaker (450 rpm) with light protection. The day after, two washing steps were conducted to eliminate unbound EVs and 15 µL of MACSPlex Exosome Detection Reagent cocktail of APC fluorescent antibodies against tetraspanins (CD9, CD63, CD81) were added. The beads-EVs solution was incubated for 1h at room temperature (RT) with light protection on an orbital shaker (450 rpm). The samples were then washed and incubated at RT, protected from light, on an orbital shaker for 15 min followed by a wash at

3000× g for 5 min. A total of 150 µL of the samples were transferred in flow cytometry tubes and detected using the BD FACS Celesta flow cytometer. The beads-EVs solution without the APC-tetraspanins antibodies was used as control. Results were normalized on the mean fluorescence intensity (MFI) for every sample.

2.5 3D PATIENT DERIVED-CRC MODEL (3D-PCRC)

CRC tissue was obtained at the edge of infiltrating neoplasia. Decellularization process was obtained by detergent-enzymatic treatment as previously described.[14] Tumor decellularized matrices (TDM) were incubated overnight with growth medium containing Primocin antibiotic (InvivoGen, Kampenhout, Belgium) at 4°C. To normalize the intra-sample variability, scaffolds were cut into comparable dimensions before seeding. All matrices were then injected with 1x106 HT29, resuspended in 10 µL of collagen I (diluted 2:3 with RPMI-1640), using a 30G syringe needle. Tumor re-cellularized matrices (TRM) were initially incubated for 4 hours in the incubator at 37°C with 5% CO2. The complete medium was then carefully added and changed every two days.

2.6 COLORECTAL CANCER MATRIX TREATMENT WITH EVS

TDM were incubated overnight with 1x109 MSC-EVs before the recellularization step. The day after, following the HT29 injection, 3x109 MSC-EV were administered at 24h and then at 72h pos-injection. Five days post-seeding EV-treated or untreated matrices were either formalin-fixed and paraffin-embedded for the IHC staining or fixed in 4% paraformaldehyde (PFA) and then included in 20% glycerol for the immunofluorescence analysis. Matrices were also snap-frozen in liquid nitrogen for molecular analysis.

2.7 TRACKING ANALYSIS OF EVS IN 3D-PCRC MODEL

Fluorometric analysis was conducted on matrices treated or not with labelled EVs. Diffusion and distribution of labelled MSC-EVs in TDM and TRM was examined. Fixed whole matrices were stained with 100 ng/mL 40,6-diamidino-2-phenylindole (DAPI; Sigma-Aldrich) at 4°C for 3 hours, washed and then included in 20% glycerol in PBS 1X for confocal analysis. Matrices injected with DiI-labelled PBS (PBS-DiI) were used as control. Imaging was performed using a Leica TCS SP5 confocal system (Leica Microsystems S.r.l., Wetzlar, Germany) with a HC PL FLUOTAR 10X (NA 0.3) Dry objective. Series of x-y-z images were collected along the z-axis at 5 µm intervals through-out the sample depth. Three-dimensional reconstruction was performed using “3D Viewer” plugin of Fiji ImageJ software. Moreover, EV presence in TRM was also analysed by global fluorescence intensity (Em. 569 nm) using a microplate reader BioTek Sinergy h1 (AHSI SpA, Bernareggio, MB, Italy).

2.8 PROTEOME AND SECRETOME ANALYSIS

2.11.1 STUDY DESIGN

Proteomics analysis was organized in three parts. In part I of the study, protein cargo of MSC-EV was characterized. In part II of the study, differentially abundant proteins were investigated in TDM or TRM after EV-treatment or not. Matrix samples were divided into four groups: (i) tumour decellularized matrices, EV-untreated (TDM CTRL; n=3) or (ii) EV-treated (TDM EV; n=3); (iii) tumour recellularized matrices, EV-untreated (TRM CTRL; n=3) or (iv) EV-treated (TRM EV; n=3). In part III, the supernatants from TRM analysed in part II were examined searching for differentially abundant proteins.

2.11.2 MASS SPECTROMETRY ANALYSIS

Protein cargo of MSC-EV, TDM and TRM samples (average weight 2.4 ± 1.3 mg) and respective supernatants were analysed by mass spectrometry. In particular, proteins were extracted from (i) MSC-EV-enriched fractions, (ii) tumour matrices and (iii) supernatants. (i) MSC-EV-enriched fraction (1x1010 EV) was reduced to around 50 µL by centrifuging (4,000 x g, 4 °C) in 3,000 molecular weight cut-off concentrators (Vivaspin; Sartorius, Göttingen, Germany). The concentrate was moved to a new tube, and lysed with a lysis buffer (A45735, Thermo Fisher Scientific, Massachusetts, USA) containing protease inhibitors (87785, Thermo Fisher Scientific) and in presence of 0.1% (w/v) RapiGest SF (Waters, Massachusetts, USA). The lysate was subjected to two cycles of freeze (-80 °C) and thaw (4 °C) and sonication (2 x 60 s). The tube was then centrifuged for 20 min at 8,000 x g to remove membrane debris. (ii) Protein extraction from tumour matrices, decellularized or not, was performed according to (Naba et al. 2015 doi:10.3791/53057), starting from 2,4 (± 1,3) mg of sample. (iii) Supernatant proteins were recovered from the serum-free medium, as above described, concentrated to around 50 µL within 3,000 MW cut-off concentrators (Vivaspin; Sartorius). Protein concentration was measured with the Pierce BCA Protein Assay Kit (Thermo Fisher Scientific). Protein extracts were immediately subjected to further down-stream analyses. Isolated Proteins (100 µg) were reduced, alkylated and digested and peptides cleaned-up with the EasyPep Mini MS Sample Prep Kit (Thermo Fisher Scientific) according to the manufacturer's protocol. Three biological replicates were analysed per group. The peptide mixtures were then analysed with LC-MS/MS, using a Q-Exactive Plus Hybrid Orbitrap mass spectrometer equipped with a UHPLC Vanquish (Thermo Fisher Scientific). Individual samples were analysed in duplicate. Each tryptic peptide sample was fractionated in a XBridge Peptide BEH C18 column (3.5 µm 2.1 x 150, Waters, Sesto San Giovanni, Milan, Italy) at a flow rate of 200 µL/min using 0.1% formic acid/acetonitrile gradient (eluent A: 0.1% formic acid in ultrapure water; eluent B: 0.1% formic acid in acetonitrile) over a period of 61.5 min, and spray onto the mass spectrometer using an heated electrospray source probe in positive mode (Thermo Fisher Scientific). Acetonitrile, formic acid (FA) and water, all LC-MS grade, were purchased from Sigma Aldrich Srl (Milan, Italy). The mass spectrometer was run in the data-dependent mode with positive polarity at electrospray voltage of 3.52 kV and capillary temperature 325 °C. Full scan MS spectra (m/z 375-1500) were acquired followed by MS/MS scans on the top 10 intense ions, applying a dynamic exclusion window of 30 seconds. Label-free quantification (LFQ) and database search were done with Proteome Discoverer software (version 2.5.0.400) using the Sequest search engine against the human database (UniProt release 2022_02) with the

following settings: 1) two max missed cleavage sites allowed, 2) precursor mass tolerance 10 ppm, fragment ion mass tolerance 0.02 Da, 3) cysteine carbamidomethylation as static modification and 4) methionine oxidation as dynamic modification. The false discovery rate (FDR) was set to 0.01. Only proteins identified with a false discovery rate (FDR) medium (5%) or high (1%), a Sequest Score ≥1 and a p-value <0.05 were considered. All potential contaminants coming from culture media were filtered. The abundance ratio (or fold change, FC) of statistically significant proteins was calculated as the ratio of the average LFQ intensities between the two matched groups. Proteins differing in abundance between the two groups were defined as those with a FC≥2 (FC Log2≥1) (proteins increasing in abundance) or a FC≤2 (FC Log2≤-1) (proteins decreasing in abundance).

2.11.3 PROTEINS FUNCTIONAL ANNOTATION

The functional annotation of differentially abundant proteins (p <0.05) was done with DAVID 6.8 (https://doi.org/10.1038/nprot.2008.211) Gene Ontology (GO) biological processes associated with the proteins were evaluated (p <0.01, Fisher's exact test). Proteins identified in the MSC-EVs were searched for the top 100 proteins released by ExoCarta (http://exocarta.org). A qualitative comparison of identified proteins was performed with Venn diagram [http://bioinformatics.psb.ugent.be/webtools/Venn/], to evidence proteins either shared by the interrogated group or unique.

2.9 IMMUNOHISTOCHEMISTRY AND IMMUNOFLUORESCENCE

Tissue samples were formalin fixed and paraffin embedded. The tissue sections (5 µm thick) were stained with Haematoxylin & Eosin (H&E; Bio Optica), Masson trichrome (aniline blue kit; Bio Optica), Alcian blue stain (pH 2.5 kit; Bio Optica) and Van Gieson trichrome (Bio Optica) for elastic fiber and connective tissue, Silver Stain (Bio Optica), Periodic Acid Schiff (PAS; Bio Optica), anti-collagen IV (1:100, Dako), and anti-Defensin alpha 3 antibody - C-terminal (1:100, Abcam) according to manufacturer's instruction. Immunohistochemical staining was automatically performed using the Bond Polymer Refine Detection kit in the BOND-MAX system (Leica Biosystems). Apoptosis was evaluated using the TUNEL assay (ApopTag Plus Peroxidase in Situ Apoptosis Detection Kit, Millipore) as described by the provider but modifying the digestion time to 5 minutes. For immunofluorescence analysis, in selected experiments TDM sections were incubated with primary antibody against Laminin (1:100, Sigma), then slides were washed and incubated with labelled Alexa Fluor secondary antibody (1:200, Thermo Fisher Scientific). Finally, nuclei were counterstained with fluorescent mounting medium plus DAPI. For each specimen, random pictures were collected with a direct microscope.

2.10 QUANTITATIVE REAL TIME PCR

TRM were weighed, then cut into smaller pieces and digested using Proteinase K (5 mg/ml) for 10 minutes at 37°C. After incubation, Trizol LS (Thermo Fisher Scientific) was added, and the samples were homogenized using 0,15 µl latex beads (Tissue Lyser II, Qiagen). Total RNA was isolated using the miRNeasy MINI kit (Qiagen) according to the manufacturer's protocol.

Total RNA (150 ng) was reverse-transcribed, and levels of specific transcripts were assessed by quantitative real time PCR (RT PCR). Primers were purchased from MWG-Biotech (Eurofins Scientific, Brussels, Belgium). Five ng of cDNA, 200 nM of specific primers and 1X SYBR Green PCR Master Mix were run on a StepOne Real Time System and data were analysed by Quant Studio 7 Pro Design and Analysis Software (all from Thermo Fisher Scientific). The amplification reaction was conducted in a final volume of 20 µl using 4 µl of cDNA, TaqMan ® Universal PCR Master Mix 1X (Applied Biosystems) and specific TaqMan ® Gene Expression Assay 1X (Applied Biosystems): Hs04260396_g1 for KI-67 and Hs00832876_g1 for BAK1. Glyceraldehyde-3-Phosphate Dehydrogenase (GAPDH) expression was used to normalize the cDNA inputs.

2.11 SCRATCH ASSAY

Scratch assay was performed to evaluate the biological activity of extracted TISSUE-EVs extracted from 3 different patients with same TNM classification. The assays were performed on CRC cell line Caco2. Caco2 cells (75k cells/well) were seeded in a 12-well plate and grown for 3 days to confluence. On the 3rd day, the scratch was performed using a pipette tip and the condition was added. Different conditions have been tested: 0% FBS (negative control), 10% FBS (Positive control), treatment with HC-TISSUE-EVs (100k EVs/cell) and treatment with CRC-TISSUE-EVs (100k EVs/cell). The imagines were acquired at 3 different time points (0h, 16h, 36h) using a Nikon TE2000E inverted microscope (Nikon, Tokyo, Japan). 3 images were taken per condition. Image analysis was performed with the ImageJ software v.1.53c. The data from three independent experiments were expressed as the mean ± SD of tube length in arbitrary units per field. The results are expressed as scratch healing (%), considering the distance between the cells border at 0h as 0%.

2.12 STATISTICAL ANALYSES

All graphs and statistical analysis were performed using GraphPad Prism Software v.9 (GraphPad Software Inc., La Jolla, CA, USA) and IBM SPSS Statistics 26 (IBM Corp, Armonk, NY). Outlier were excluded performing ROUT outlier test. For comparison between coupled experimental groups two-sided Student's t-tests (for parametric dataset) and Mann-Whitney test (for non-parametric dataset) were used. One-way ANOVA with Bonferroni's post-test (for parametric dataset) and Kruskal-Wallis's test with Dunnett post-test (for non-parametric dataset), was performed for multiple comparisons. A p-value < 0.05 was considered statistically significant. For each significant marker, receiver operating characteristics (ROC) curves were analysed to assess the area under the curve (AUC). Odds ratios (ORs) were calculated by univariate logistic regression.

CHAPTER 3: RESULTS

3.1 EVs ISOLATION AND CHARACTERIZATION

3.1.1 TISSUE-EVs

Hematoxylin and Eosin confirmed the structure of tumor fresh tissue (HC-TISSUE, Fig. 6A) and fresh colon healthy mucosa (CRC-TISSUE, Fig.6B).

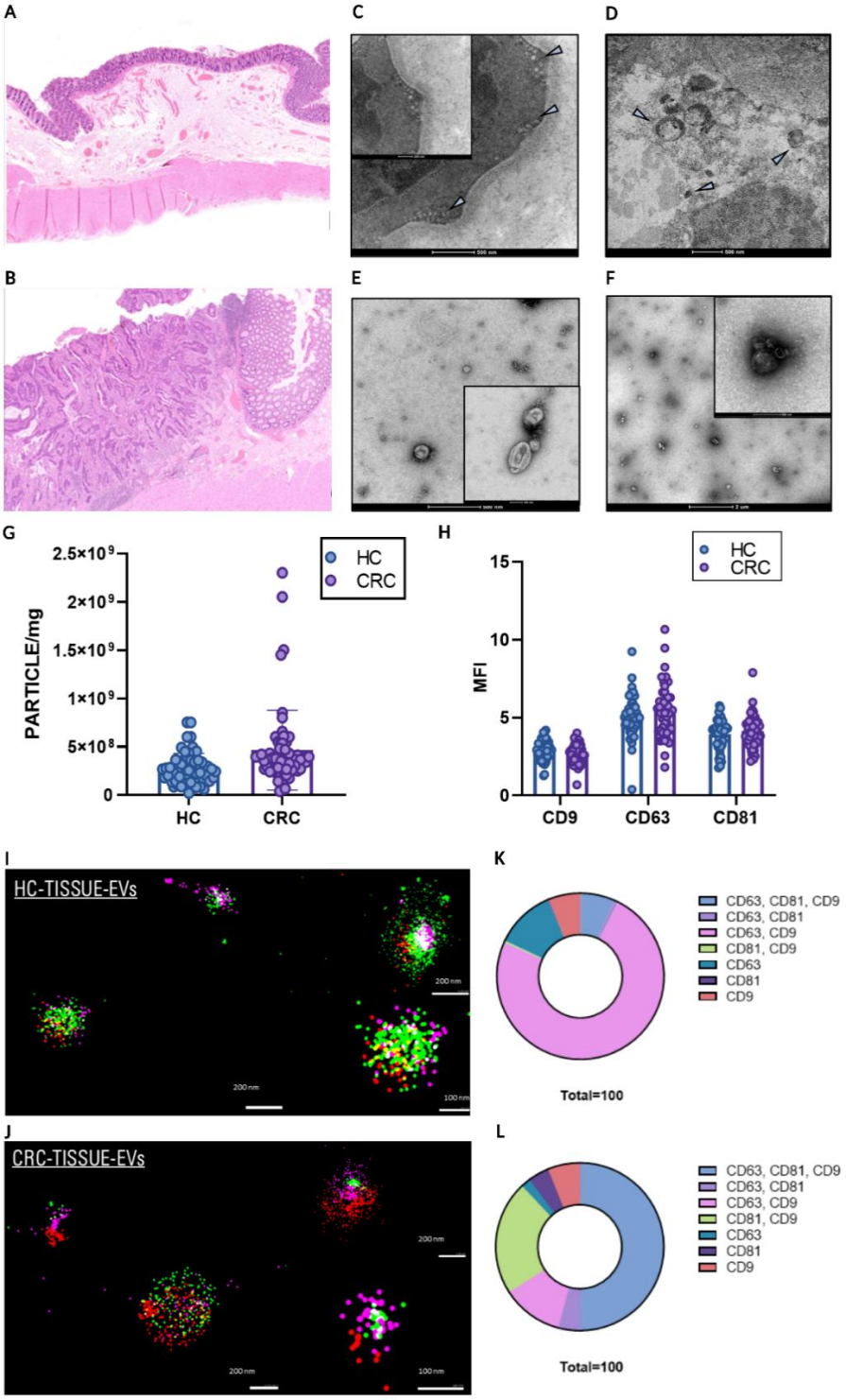

Figure 6 - TISSUE-EVs from tumor and healthy mucosa characterization. A-B: Hematoxylin & eosin staining of healthy (HC, A) and tumor (CRC, B) fresh tissue. C-D: TEM images of EVs trapped in healthy (HC, C) and tumor (CRC, D) fresh tissue. E-F: TEM images of HC-

TISSUE-EVs (E) and CRC- TISSUE-EVs (F) with small (100nm) and large (500nm) EVs. G: Concentration of EVs extracted from fresh healthy and tumor tissues. H: Tetraspanins mean expression in TISSUE-EVs of all samples in the study (n=123) quantified via bead-based flow cytometry using MACSPlex assay. I-J: Representative super-resolution images of small (100nm) and large (500nm) tetraspanins triple positive in HC-TISSUE-EVs (I) and CRC-TISSUE-EVs (J). K-L: Tetraspanins co-expression percentage in HC (K) and CRC (L) TISSUE-EVs.

The presence of the EVs in both HC and CRC tissue (respectively Fig.6C and Fig.6D) with TEM analyses. Equally, the success of the extraction protocol was confirmed by observing the integrity of both HC-TISSUE-EVs and CRC-TISSUE-EVs (respectively Fig.6E and Fig.6F). Analyzing the shape of TISSUE-EVs, two different populations were identified: one small population around 100nm and one large population around 500nm, for both HC-TISSUE-EVs (Fig. 6E) and CRC-TISSUE-EVs (Fig.6F). The concentration and size of EVs was assessed by NTA. The extraction rate of CRC-TISSUE-EVs (4.63E+08 particle/mg), was higher than HC-TISSUE-EVs (2.63E+08 particle/mg) (Fig.6G). The presence of tetraspanins (CD9, CD63 and CD81) was assessed, through bead-based cytofluorimetric and through super-resolution microscopy. MACsplex detected CD9, CD63 and CD81 in both HC-TISSUE-EVs and CRC-TISSUE-EVs, with CD63 showing the highest expression (Fig. 6H). Single vesicle analysis confirmed the homogenous distribution of these molecules on both healthy and tumor vesicles (Fig.7G). Furthermore, super-resolution microscopy confirmed the presence of small and large populations of vesicles in both HC and CRC-TISSUE-EVs (Fig.6I-J). Evaluating the tetraspanins co-expression, the double positive CD63 and CD9 were the main EVs population in HC-TISSUE-EVs (Fig. 6K) while the triple positive were the main EVs population in CRC-TISSUE-EVs (Fig 6L).

3.1.2 ECM-EVs

The experimental plan of extraction and analyses performed for ECM-EVs is shortly described on Fig.7A. The presence of intact EVs in decellularized colorectal tissue was initially assessed by TEM, which showed EVs trapped in both normal and tumor-derived decellularized ECM (Fig. 7B and 7C). When comparing EVs isolated with different enzymatic ECM digestions, TEM analysis showed that EVs extracted using collagenase treatment retained collagen strengths on their surface, confirming their entrapment in the ECM (Fig. 7D). On the contrary, EVs extracted with proteinase K appeared rounded and completely denudated of ECM residues. This method was then chosen for further studies (Fig.7E). EV size, concentration and tetraspanins expression was subsequently assessed. NTA analysis showed no difference in the extraction rate and dimension, differently from TISSUE-EVs, between healthy and tumor decellularized tissues (Fig 7F-G). In particular, the recovery yield was 5.35 E+09 particle/ml and 4.55 E+09 particles/ml for preparations extracted from normal decellularized colon decellularized tissue (HC-ECM-EVs) and cancer decellularized colon tissue (CRC-ECM-EVs), respectively (Fig. 7F). The presence of tetraspanins (CD9, CD63 and CD81) was assessed through bead-based cytofluorimetric analysis using the MACsplex exosome kit and through super-resolution microscopy. CD9, CD63 and CD81 were detected in both HC- and CRC-ECM-EVs, with CD63 showing the highest expression among tetraspanins as described for TISSUE-EVs (Fig. 7J). Single vesicle analysis confirmed the homogenous distribution of these molecules on both healthy and tumor vesicles. Triple, double and single positive EVs were detected for each tetraspanins (Fig. 7K-L).

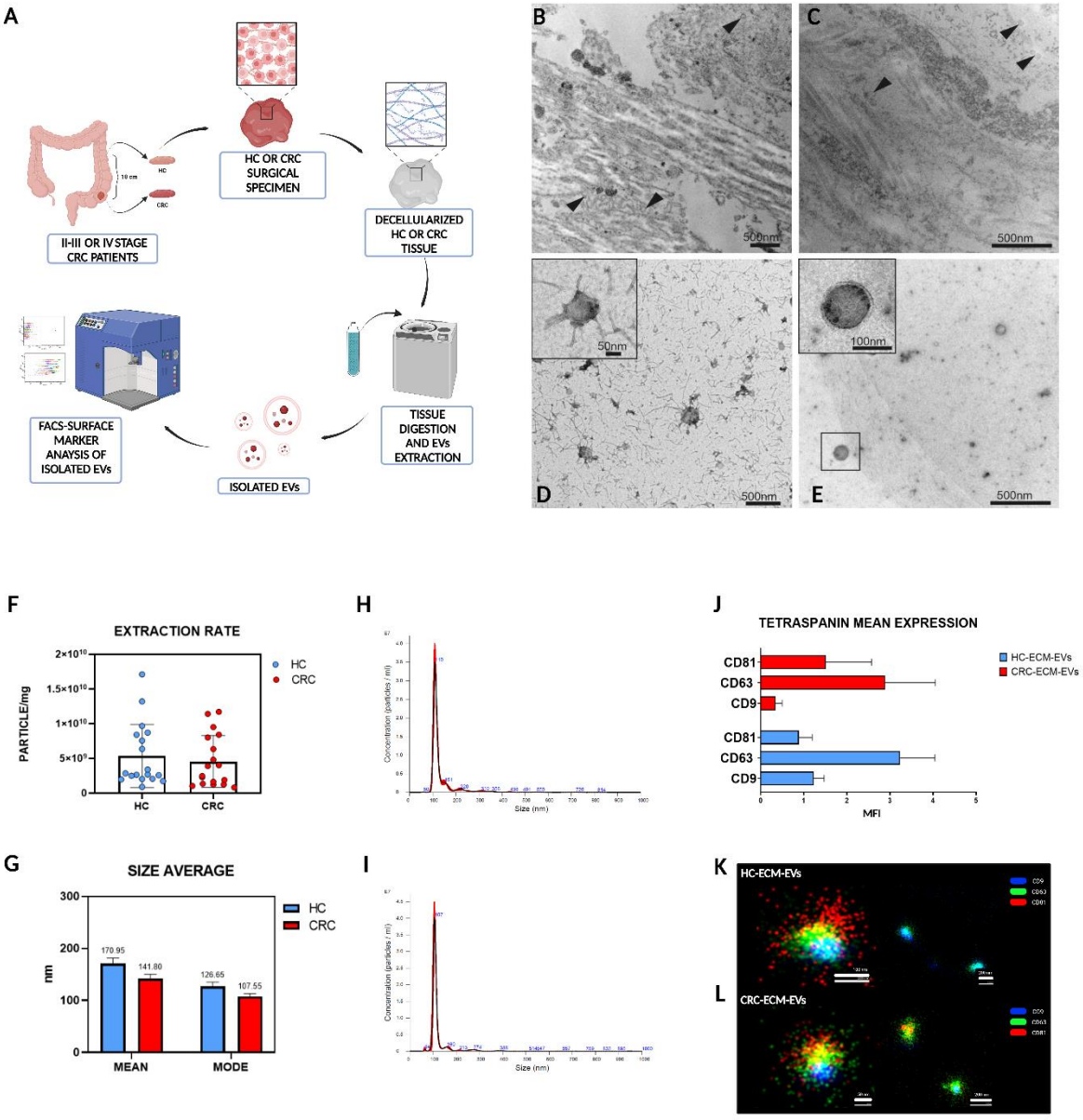

Figure 7 - ECM-EV extraction from tumor and healthy mucosa and characterization. A: Schematic representation of the study). B-C: TEM images of EVs trapped in healthy (HC-ECM-EVs, B) and tumor (CRC-ECM-EVs, C) decellularized tissue. D-E: TEM images of ECM-EVs extracted with Collagenase (D) and Proteinase K (E). F.G Concentration of EVs extracted from decellularized healthy and tumor tissues and their size distribution. H-I: Representative NTA graph of HC-ECM-EVs (H) and CRC-ECM-EVs (I). J: Tetraspanins mean expression in ECM-EVs of all samples in the study (n=23) quantified via bead-based flow cytometry using MACSPlex assay. K-L: Representative super-resolution images of triple (left) and double (right) tetraspanins positive ECM-EVs. Directly from accepted paper: Profile of matrix-entrapped extracellular vesicles of microenvironmental and infiltrating cell origin in decellularized colorectal cancer and adjacent mucosa – Tassinari S. et al.

3.1.3 MSC-EVs

MSC-EVs were first analyzed using Nanoparticle Tracking Analysis (NTA) showing an amount of 4196 EVs/cell. EVs presented a homogeneous distribution with a mode mean diameter of 97.76 nm (Figure 8A). In Figure 8B, the presence of surface exosome marker CD63 confirms the nature of the vesicles in our preparation. Moreover, TEM representative images showed rounded structures between 50 and 150 nm diameter, consistent with the expected size distribution of small EVs population (Figure 8C). Semiquantitative analysis of tetraspanins

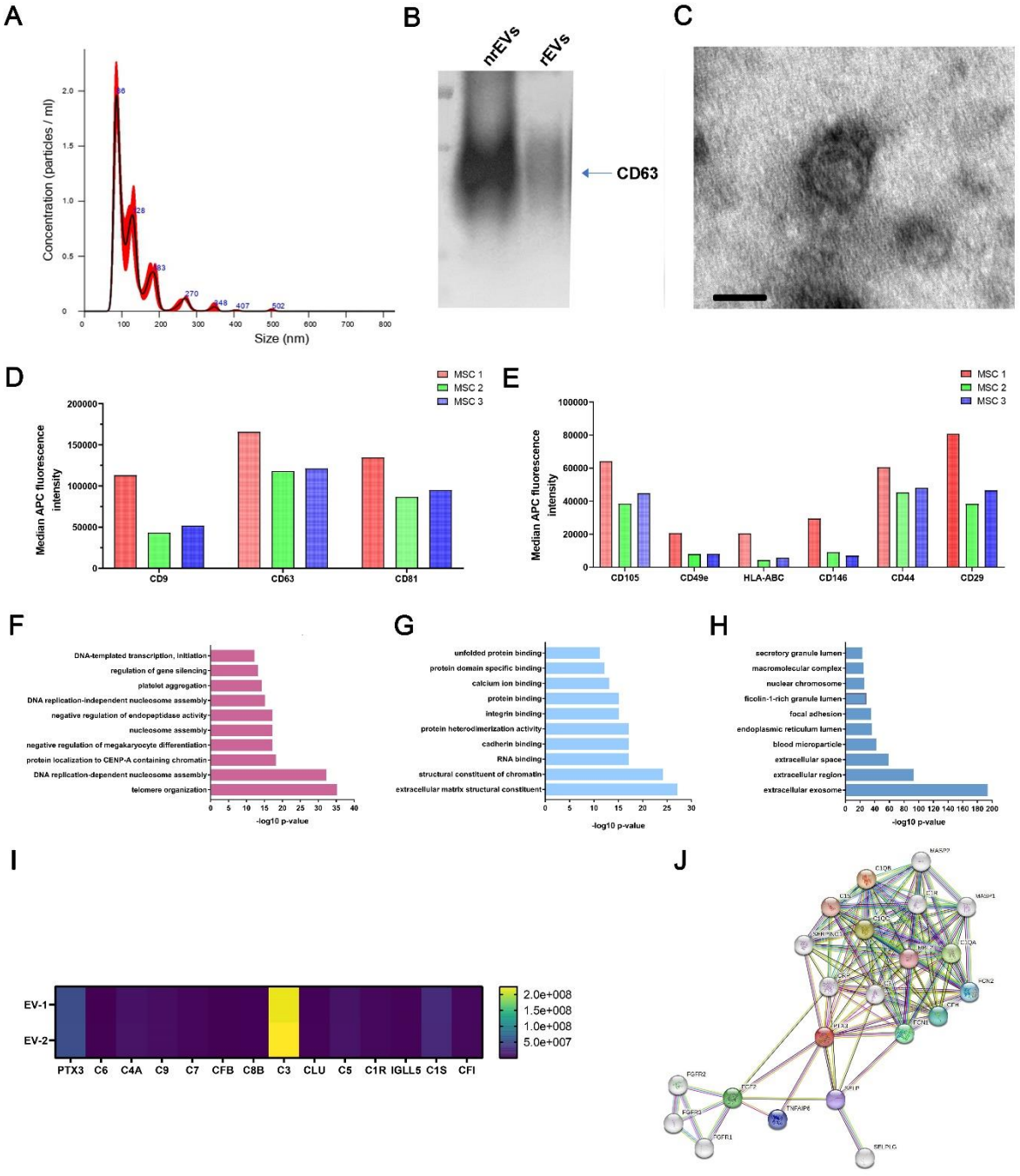

Figure 8 - Characterization of EVs isolated from MSCs. A: Size distribution of MSC-EVs using Nanoparticle Tracking Analyses. B: Western blot analysis of protein expression of exosome-associated tetraspanins CD63 in not reduced (nrEVs) or reduced conditions (rEVs). C: Transmission Electron Microscopy representative image of isolated MSC-EVs, scale bar=100 nm. D-E: Multiplex flow cytometry analysis of EVs markers, such as tetraspanins (D) and mesenchymal markers (E). The x-axis shows the protein marker profile, whereas the y-axis represents the normalized Median APC fluorescence intensity. F-H: Functionally annotation using DAVID Bioinformatics Resources of 379 EV proteins identified using mass spectrometry: (F) Biological processes; (G) Molecular functions; (H) Cellular complement. I: Heatmap of Complement and complement-related proteins identified in two different preparations of MSC-EVs. The relative abundance of proteins belonging to the Complement pathway were calculated as the intensity of the precursor ion peak. J: Complement and complement-associated protein interaction as predicted from STRING database. Directly from submitted paper: Reconstructed colorectal cancer model to dissect the anti-tumor effect of mesenchymal stromal cells derived extracellular vesicles – D'Angelo E. et al.

levels in the MSC-EVs were performed using the MACSPlex exosome kit, a bead-based cytofluorimetric analysis. All the MSC preparation tested preserved the expression of the three tetraspanins, with a higher level for CD63 and CD81 over the CD9 molecule (Figure 8D). The

expression of mesenchymal markers, in MSC-EVs was also assessed[93]. The results showed the positivity of MSC-EVs for CD29, CD44, CD146, CD49e, CD105 and HLA-ABC (Figure 8E). Proteomic analysis of MSC-EVs was performed to fully characterize both the membrane and cargo protein fractions. Label-free untargeted LC-MS/MS-based proteomic analysis identified 379 proteins within the EVs (FDR<0.01). The interrogation of ExoCarta database revealed that 53 of the 100 most expressed proteins detected in MSC-EVs have already been identified in exosomes from various human samples. We orthogonally confirmed the cytofluorimetry data by detecting the presence of CD63 and CD81 markers in LC MS/MS data. The 379 EV proteins were functionally annotated using DAVID Bioinformatics Resources. The GO enrichment analysis for the most represented biological processes were listened in (Figure 8F) and related to nuclear function and DNA regulation. The most significant molecular functions were mainly connected to ECM constituent and cell adhesion molecules (Figure 8G). While the most significant cellular components were extracellular space and exosome (Figure 8H). Interestingly, among the significant biological processes we also identified those related to regulation of apoptotic process (GO:0042981) and ECM organization (GO:0030198). A strong over-representation of the Complement pathway with a total of 13 proteins annotated was observed and associated with complement activation (GO:0006956), complement activation alternative pathway (GO:0006957) and complement activation classical pathway (GO:0006958) (Figure 8I-J). The relative abundance of proteins belonging to the Complement pathway in the heatmap were calculated, in two independent samples, as the intensity of the precursor ion peak (Figure 8I).

3.2TUMOR DERIVED EV SURFACE MARKER PROFILE:

The expression of different surface markers on EVs extracted from fresh or decellularized tissues, possibly related to the different cell origin, was assessed using the MACSplex assay, evaluating 37 different surface proteins. Data were normalized to the mean fluorescence intensity of the sample.

3.2.1 TISSUE-EVs

The surface marker expression of EVs extracted from biopsy and surgical HC or CRC samples and diverticulitis surgical specimen is summarized in the heatmap (Fig.9A). By averaging the expression of each marker among all healthy and tumour samples, we identified the most highly expressed markers in both HC-TISSUE-EVs and CRC-TISSUE-EVs. Some markers were found to be characteristic of the colorectal epithelium as they were expressed indistinctly by all vesicles extracted from the different tissue types. We identified as commonly expressed TISSUE-EVs marker, stem cell marker (CD133-1 and CD24) and epithelial marker (CD326) (Fig.9A). Moreover, comparing HC- vs CRC-TISSUE-EVs, tumor EVs showed a significantly increased expression of platelet markers (CD42a, CD62p, CD142 – Fig.9B), myeloid markers (CD11c, CD14, HLA-DR– Fig.9C), lymphoid markers (CD24, CD40, CD86– Fig.9D) and angiogenesis marker (CD31– Fig.9E). Only CD56, NK marker, was found to be strongly decreased probably due to immune-escape mechanism (Fig.9D). On the other hand, HC-TISSUE-EVs significantly expressed higher levels of cell activation markers (CD69, HLA-ABC– Fig.9F) and tissue specific markers (CD29, CD44, CD146– Fig.9G).

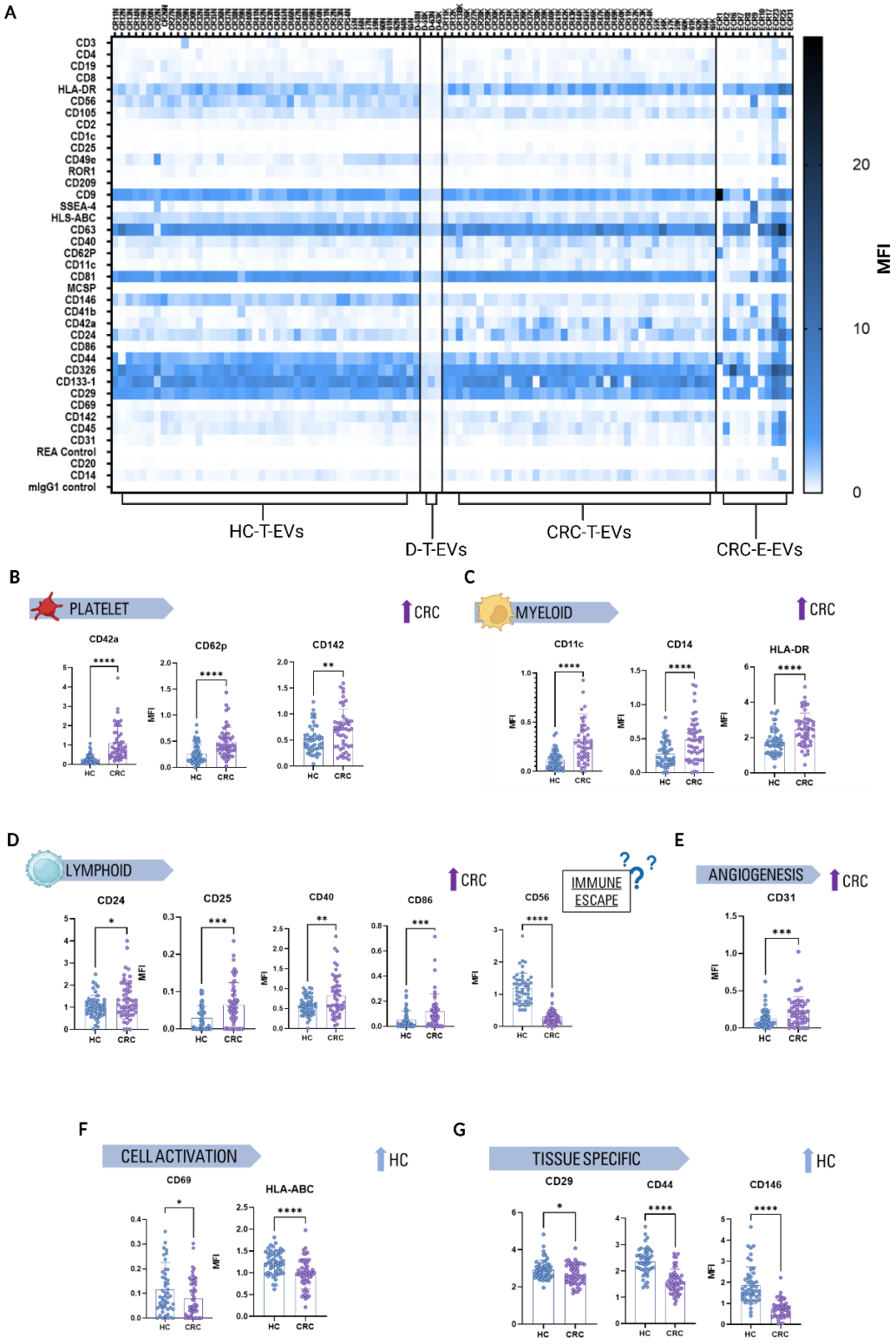

*Figure 9 - Overall comparison of marker expression in Tissue derived EVs. A: Mean heat map for surface markers EVs extracted from healthy tissue (HC-T-EVs, 56), Diverticulitis tissue (D-T-EVs, 4), CRC tissue (CRC-T-EVs,52) and Endoscopic CRC tissue (CRC-E-EVs,11). B-G: Histogram depicting differentially expressed markers between HC- (52) and CRC-TISSUE-EVs (52). Data are expressed as Mean Fluorescence Intensity (MFI). Outliers were excluded and Multiple T-test was performed: *=p<0.05, **=p<0.01, ***=p<0.001, ****=p<0.0001.*

The sensitivity and specificity of the analyzed markers were evaluated with ROC curves, and results are reported in Fig. 10A.

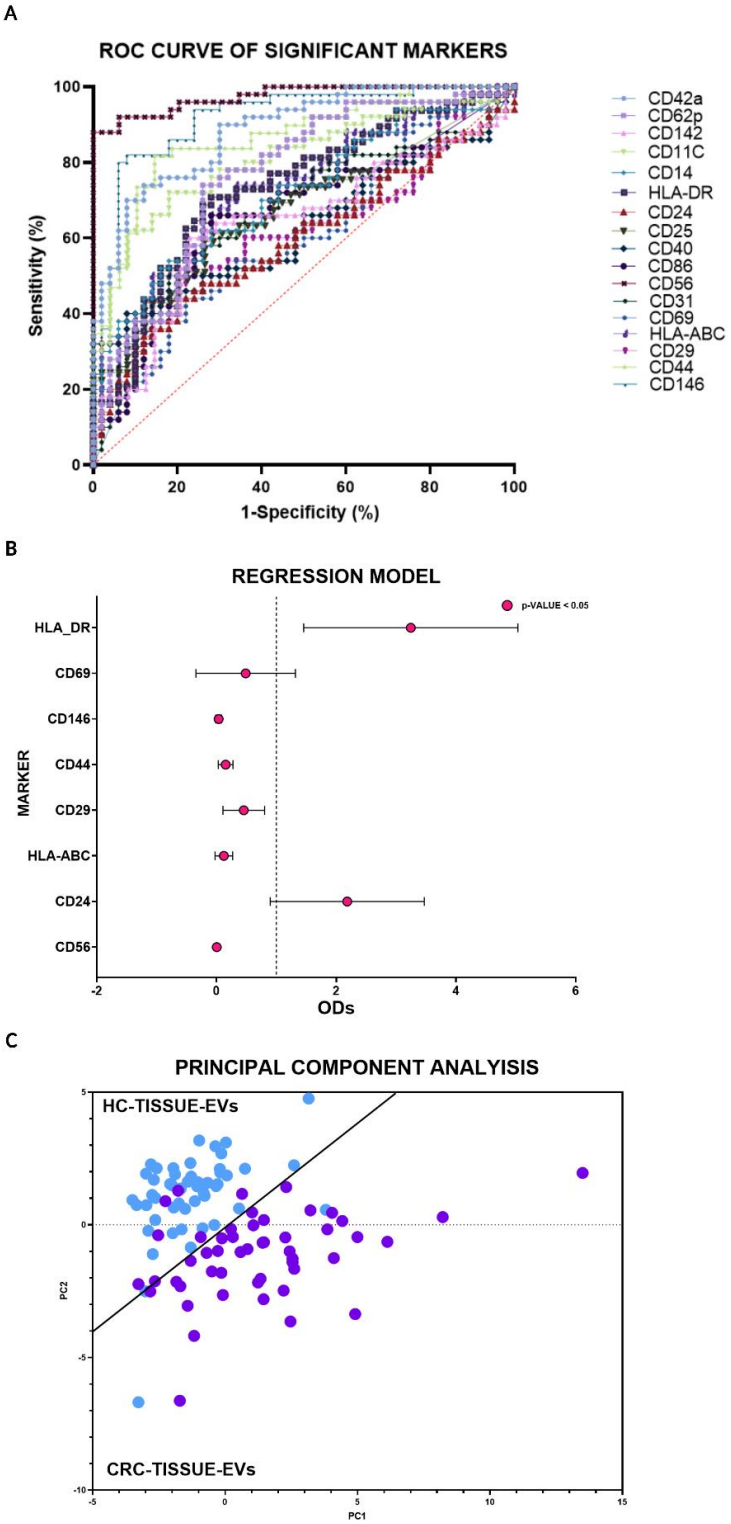

Figure 10 - Diagnostic value of significantly different markers between HC- and CRC-TISSUE-EVs. A: ROC curve of significantly different marker with AUC > 0.5 and =p<0.05. B: Regression model performed on the 37 different antigens; odds are reported for significant antigen together with its 95% CI. C: Principal component analysis performed on the 37 markers. The diagonal line highlights the different distribution of HC- and CRC-TISSUE-EVs. Directly from accepted paper: Profile of matrix-entrapped extracellular vesicles of microenvironmental and infiltrating cell origin in decellularized colorectal cancer and adjacent mucosa Tassinari S. et al.

3.2.2 ECM-EVs

The analysis showed the presence within both normal and tumor ECM-EVs of markers mainly related to immune, epithelial, and platelet origin. In CRC-ECM, EVs appeared to mainly express immune markers (CD3, CD56 and HLA-DR) (Fig. 11A and B). In the surrounding healthy colon mucosa, CD3 and CD56, were also highly expressed. Comparing CRC- and HC-ECM-EVs, those isolated from decellularized normal tissue adjacent to the tumoral lesion (10 cm far) showed a significantly higher expression of CD9, CD40 (inflammatory marker), CD42a (platelet marker), CD24 and CD326 (epithelial markers), with respect to the tumor counterpart (Fig. 11B). At variance, no marker was overexpressed in tumor ECM-EVs.

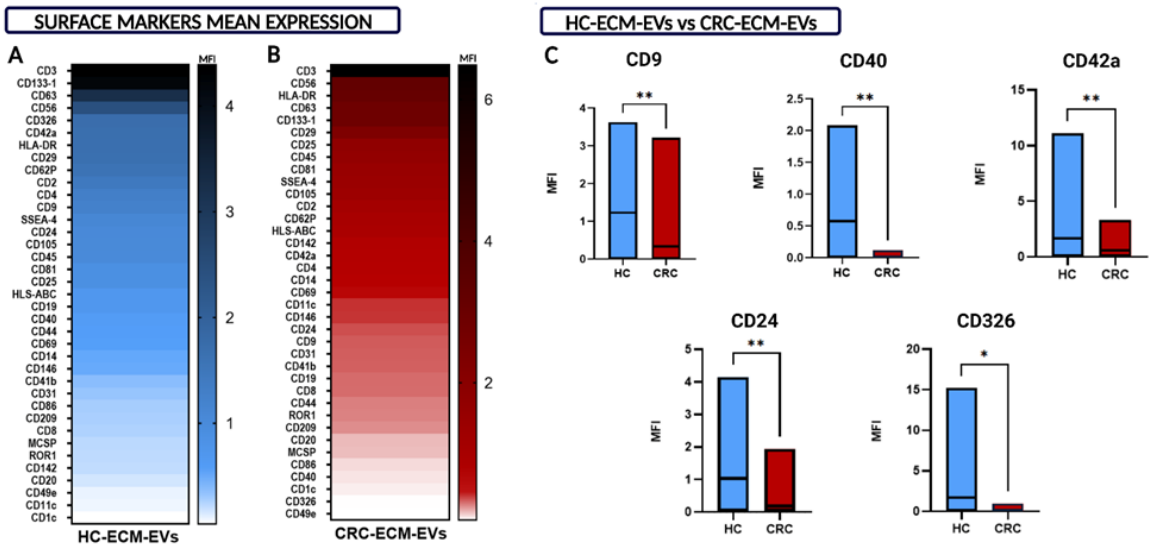

*Figure 11 - Overall comparison of marker expression in HC- and CRC-ECM-EVs. A-B: Mean expression heat map for EVs extracted from healthy decellularized tissue or tumor decellularized tissue. C: Histogram depicting differentially expressed markers between HC- (23) and CRC-ECM-EVs (23). Data are expressed as Mean Fluorescence Intensity (MFI). Multiple T-test was performed: *=p<0.05, **=p<0.01, ***=p<0.001, ****=p<0.0001. Directly from accepted paper: Profile of matrix-entrapped extracellular vesicles of microenvironmental and infiltrating cell origin in decellularized colorectal cancer and adjacent mucosa Tassinari S. et al.*

Normal and CRC-ECM-EVs were further divided in relation to the tumor stage, in stage II-III ECM-EVs (n=11) and those stage IV ECM-EVs (n=12). Interestingly, no significant differences were observed between II-III CRC-ECM-EV and their corresponding HC, indicating that the observed overall differences, shown above in Fig. 11, were restricted to stage IV. Indeed, in those samples, the profile of EVs obtained from healthy decellularized colon mucosa showed an overexpression in CD24, CD40, CD42a, and CD326, with respect to the stage IV decellularized tumor (Fig. 12A). In addition, CD44 (adhesion marker) and CD49e, (platelet marker), were also increased in the decellularized mucosa compared to stage IV decellularized tumor (Fig. 12A).

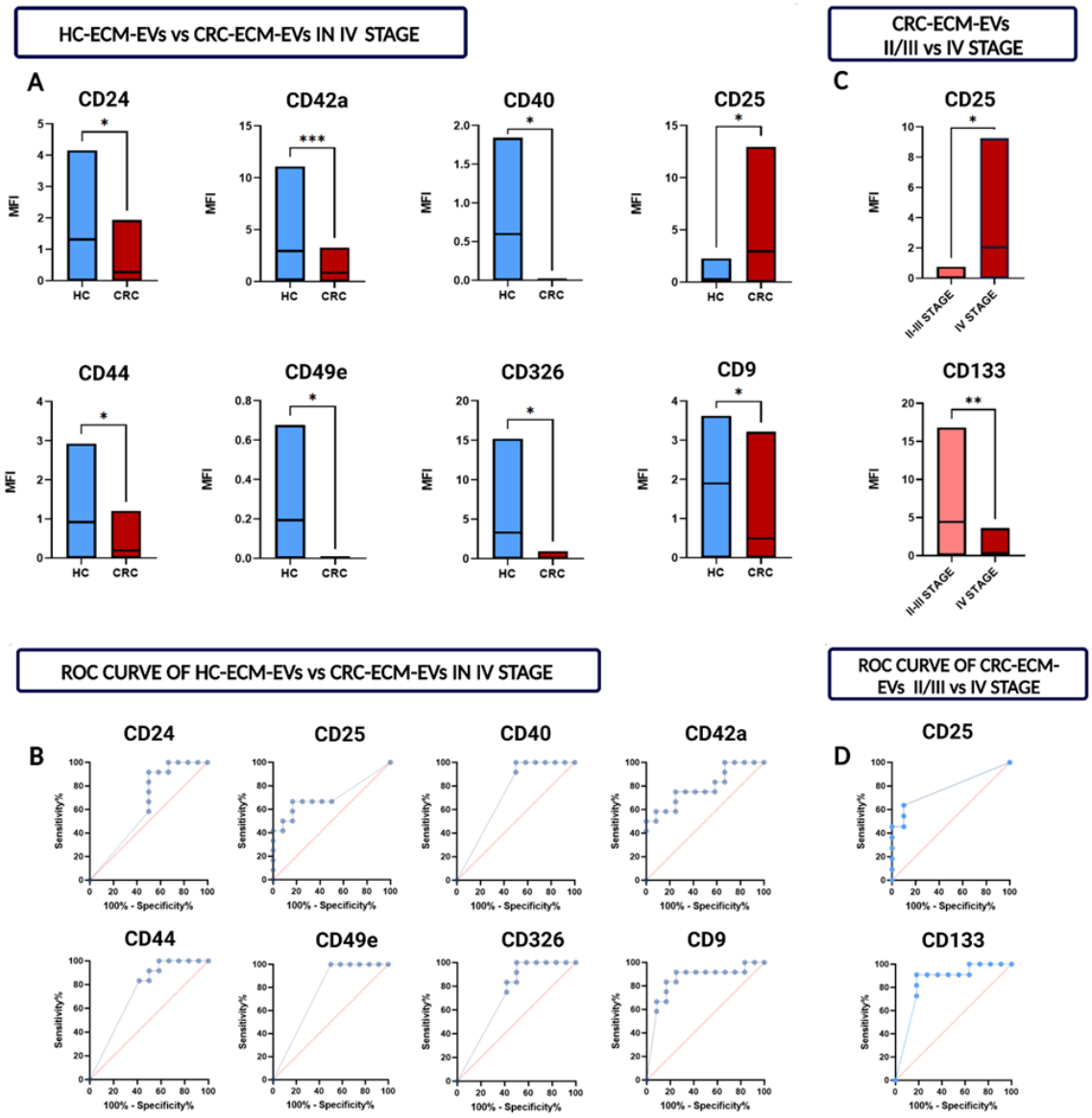

*Figure 12 - Comparison of ECM-EVs from healthy and colon tumors according to tumor stage. A-B: Histogram depicting the significant different expression of multiple markers between HC-ECM-EVs (12) and CRC-ECM-EVs (12) in stage IV CRC patients. together with corresponding ROC curves. C-D: Histogram of significantly different markers obtained comparing tumor ECM-EVs in the different CRC (11 II-III stage vs 12 IV stage) stages and corresponding ROC curves. Data are expressed as Mean Fluorescence Intensity (MFI). Multiple T-test was performed: *=p<0.05, **=p<0.01, ***=p<0.001, ****=p<0.0001. Directly from accepted paper: Profile of matrix-entrapped extracellular vesicles of microenvironmental and infiltrating cell origin in decellularized colorectal cancer and adjacent mucosa Tassinari S. et al.*

The sensitivity and specificity of the analyzed markers were evaluated with ROC curves, and results reported in Fig. 12B. The CD49e, CD44, CD42a and CD40 values yielded an AUC above 0.75, separating stage IV tumor and non-tumor tissues. These results indicate a specific change in the ECM of the colon mucosa surrounding the tumor that appears restricted at the stage IV CRC, with platelet and inflammatory cell infiltration, and possibly activation of epithelial cells. The increase in platelet (CD42a, CD62p) and epithelial/stem markers (CD326, CD105, SSEA-4, CD44) was also observed when comparing ECM-EVs in mucosa from stage IV CRC with respect to stage II-III CRC (Fig.13). In addition, CD25, a marker of T-regulatory lymphocytes, was the exclusive marker overexpressed in tumor ECM-EVs at stage IV in comparison with the respective healthy mucosa (Fig. 12A). This increase was confirmed by the

comparative evaluation with the CRC-ECM-EVs at the stage II-III (Fig. 12C), suggesting that the presence of EVs from T lymphocytes expressing CD25 may characterize the stage IV CRC-ECM. In addition, CD133, a marker of colon epithelial cells[94], was lower in ECM-EVs at stage IV, suggesting the loss of the epithelial phenotype within tumor progression. The ROC curves generated from these data showed a good AUC value with a significant p-value for both (Fig. 12D).

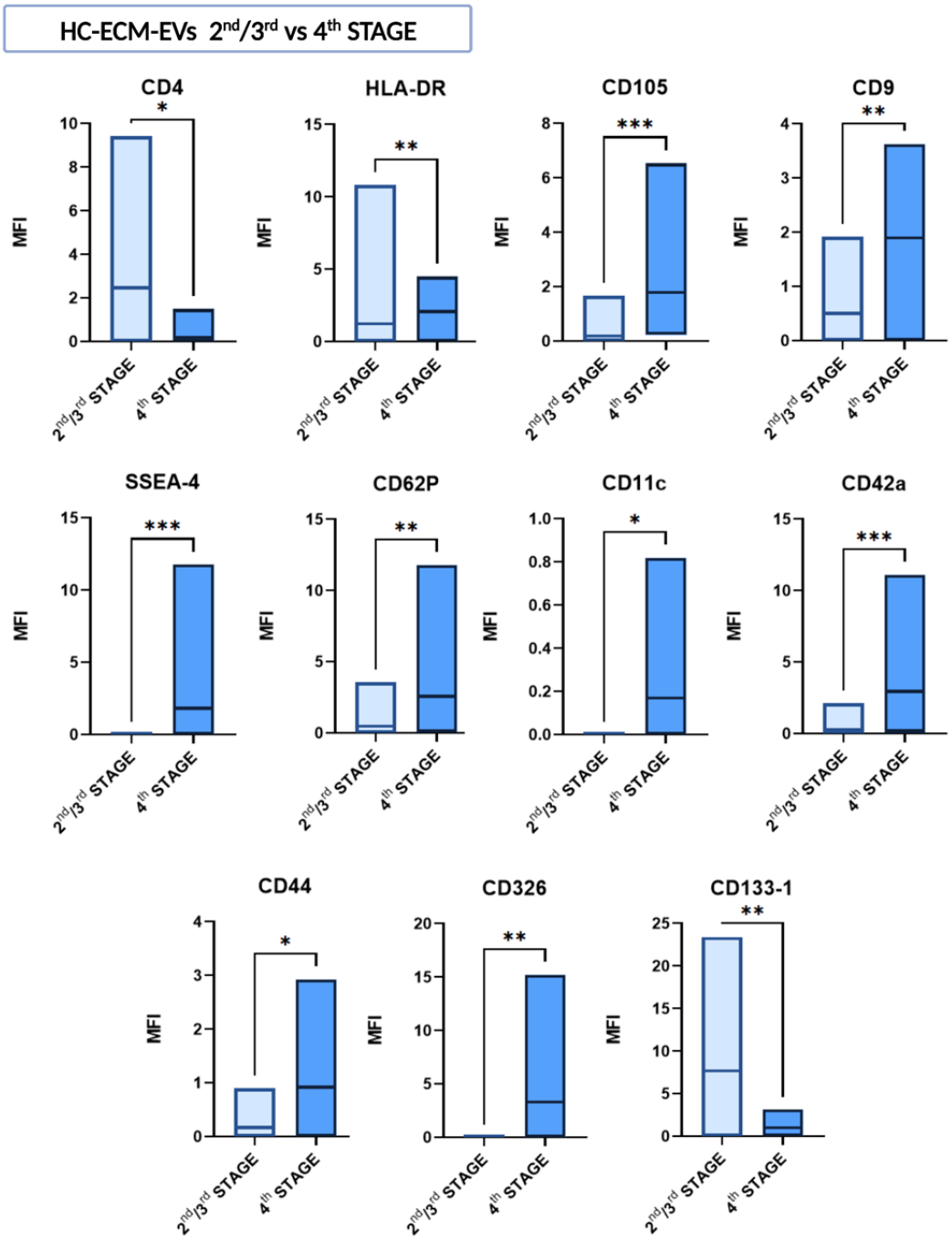

*Figure 13 - Comparison of ECM-EVs from healthy mucosa at different tumor stages: histogram depicting the significant different expression of multiple markers between II-III stage (11) vs IV- stage (12) HC-ECM-EVs. Data are expressed as Mean Fluorescence Intensity (MFI). Multiple T-test was performed: *=p<0.05, **=p<0.01, ***=p<0.001, ****=p<0.0001. Directly from accepted paper: Profile of matrix-entrapped extracellular vesicles of microenvironmental and infiltrating cell origin in decellularized colorectal cancer and adjacent mucosa Tassinari S. et al.*

Altogether, 16 EV surface antigens were identified as differentially expressed among the extracted EVs in the different tumor stages and decellularized tissue type, which include immune, platelets, or epithelial stemness-related markers (Fig. 14A). PCA performed on the significant markers in each comparison (Fig. 14B) showed a specific cluster of HC-ECM-EVs from stage IV CRC with respect to both HC-ECM-EVs from stage II-III CRC (Fig 14B) and to CRC-ECM-EVs (Fig. 14B), suggesting the presence of a subset of ECM-EVs of different origin in healthy mucosa surrounding the primary stage IV colon tumors.

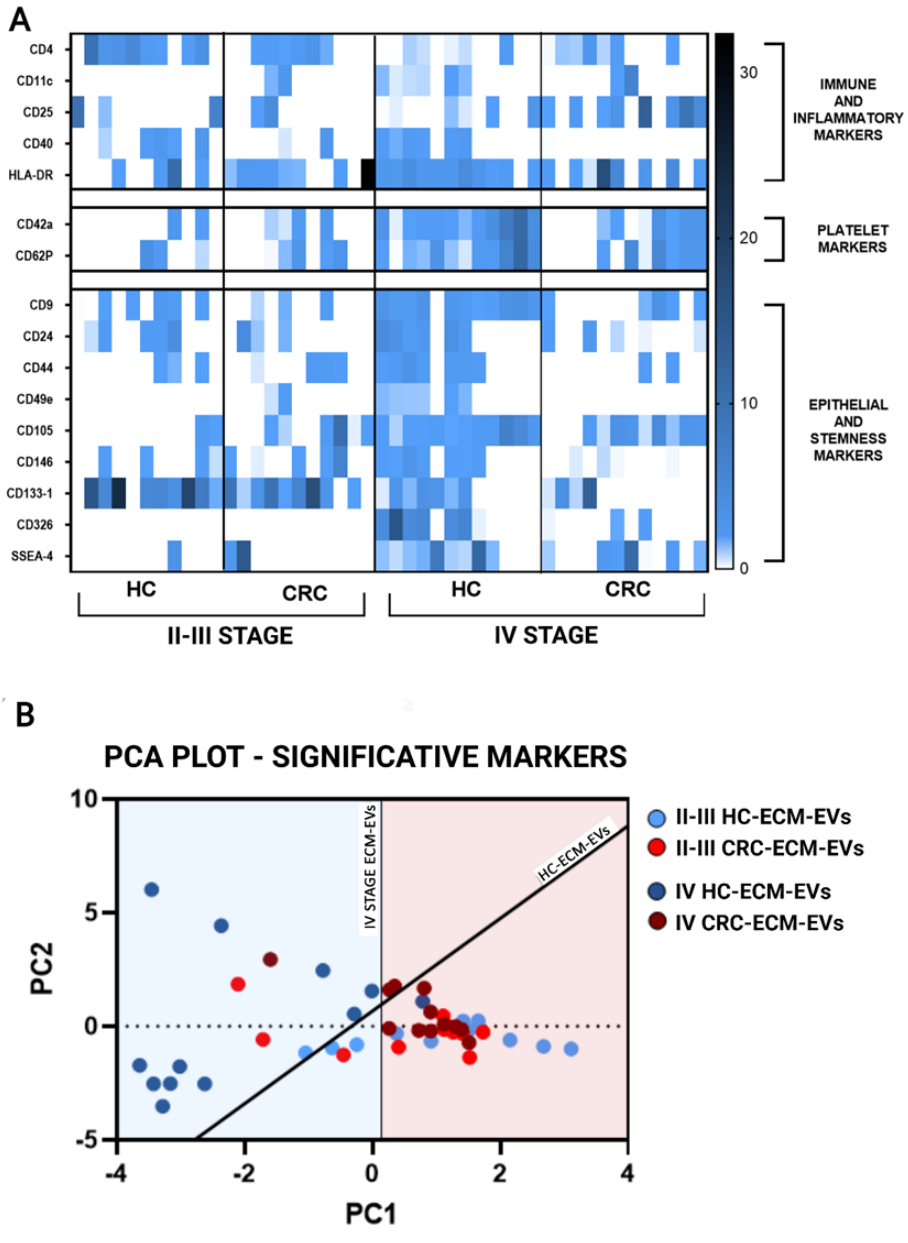

Figure 14 - Origin and distribution of the significantly different markers in HC and CRC-ECM-EVs in the different tumor stages. A: Heatmap and cellular origin of the significantly different markers. B: Principal component analysis performed on significant markers. The central line is highlighting the different distribution of IV stage ECM-EVs, separating HC vs CRC ECM-EVs. The diagonal line highlights the different distribution of HC-ECM-EVs, separating II-III vs IV stage. Directly from accepted paper: Profile of matrix-entrapped extracellular vesicles of microenvironmental and infiltrating cell origin in decellularized colorectal cancer and adjacent mucosa Tassinari S. et al.

3.3 FISIOPHATOLOGICAL EFFECT OF DIFFERENT IN CRC EVs

3.3.1 INVASION CAPACITY OF TISSUE-EVs

The biological activity of extracted TISSUE-EVs was assessed performing a scratch-healing/scratch assay. The assay was performed on CRC cell line Caco2 to understand the role of the extracted EVs in tumor invasion. Different conditions have been tested: 0% FBS as negative control, 10% FBS as Positive control and finally, the treatment with HC-TISSUE-EVs (100k EVs/cell) and with CRC-TISSUE-EVs (100k EVs/cell) (Fig.15A). The treatment with both HC- and CRC-TISSUE-EVs significantly increased the wound healing in comparison with both the controls (Fig15B). Comparing the two different treatments, CRC-TISSUE-EVs significantly improved the invasion of the wound in comparison with HC-TISSUE-EVs treatment, showing an activity improving the invasion capability of Caco2 cells (Fig.15B).

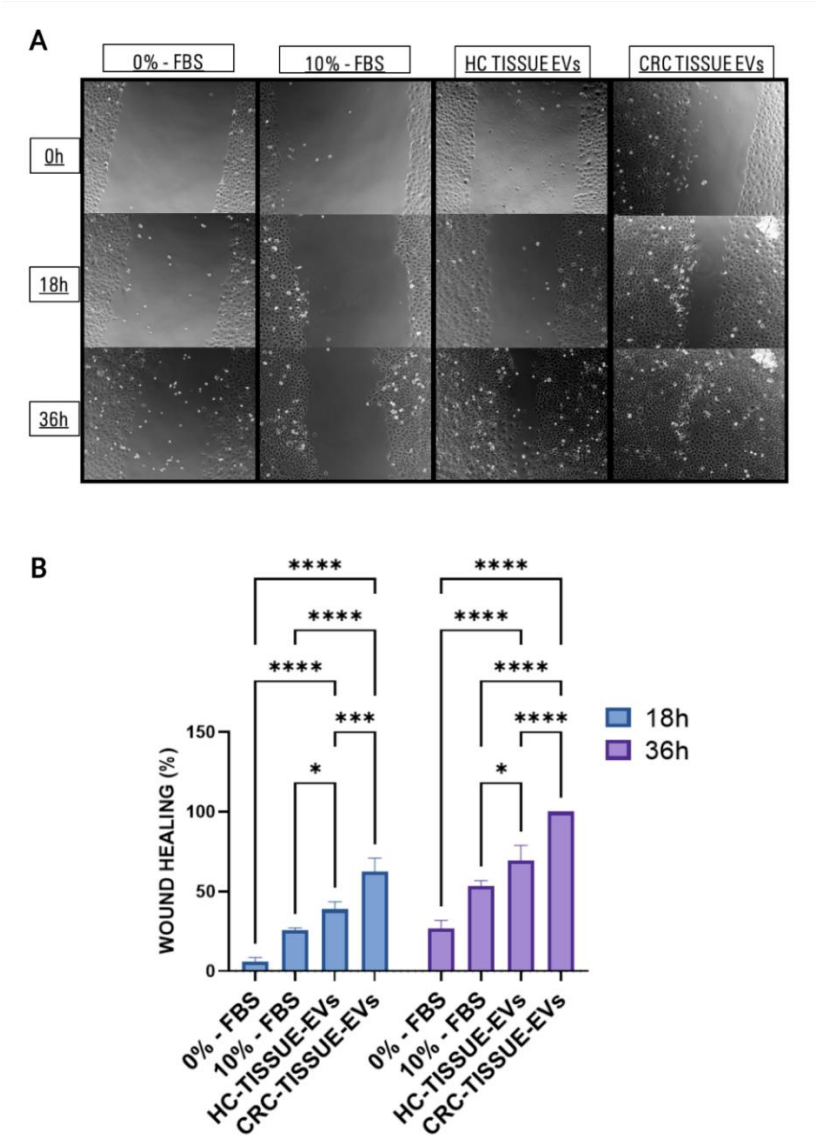

Figure 15 – Evaluation of TISSUE-EVs biological activity on Caco2 cell line. TISSUE-EVs used in the assay were extracted from HC-TISSUE and coupled CRC-TISSUE of 3 different patients with same TNM classification. The imagines were acquired at 3 different time points (0h, 16h, 36h) and every condition were performed in triplicate, 3 images were taken per condition at every time point. Image analysis was performed with the ImageJ software v.1.53c. A: Scratch assays representative images

*of the different tested conditions, acquired at different time points (0h, 18h, 36h). B: histogram representing the wound healing percentage and the statical differences between controls and EVs treatment. The data from three independent experiments were expressed as the mean ± SD of tube length in arbitrary units per field. The results are expressed as scratch healing (%), considering the distance between the cells border at 0h as 0%. One-way ANOVA with Bonferroni's post-test was performed for multiple comparisons: *=p<0.05, **=p<0.01, ***=p<0.001, ***=p<0.0001.*

3.3.2 3D PATIENT-DERIVED DECELLULARIZED MATRIX (3D-pCRC) AS A MODEL

The internalization capacity of MSC-EVs into HT29 colon cancer cell line was initially assessed. After co-incubation with DiI-labeled MSC-EVs for 24 hours, HT-29 were fixed and observed under a confocal microscopy. Our results revealed that EVs strongly entered colon cancer cells (Figure 16A) thus confirming the applicability of this cancer model to our study.

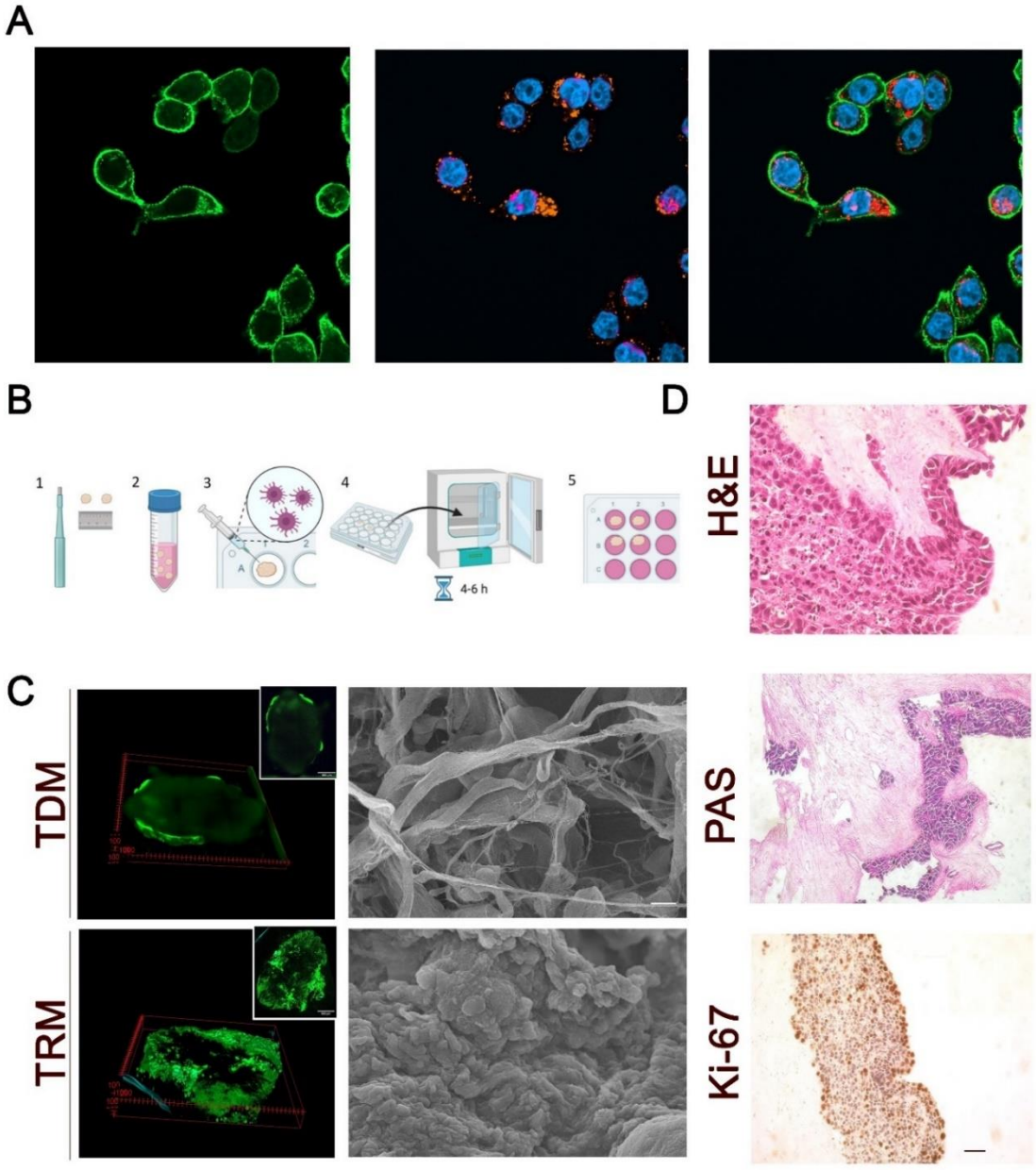

Figure 16 - Internalization of MSC-EVs of HT29 in 2D and generation of the 3D-pCRC model. A: HT29 (left panel, Phalloidin, green) uptake of MSC-EVs (middle panel, DiL, red) in conventional 2D culture. Cell nuclei were counterstained using DAPI. Scale bar=100µm. B: Schematic representation of 3D-pCRC model development: 1. Decellularized CRC biopsies were uniformly sized using a punch; 2. pre-rinsed in culture medium for 2h in incubator; 3. cell line was injected using a 30G syringe needle; 4. dry 3D-pCRC was cultivated in the incubator for 4-6h and finally 5. Culture medium was added. C: Left

panels, immunofluorescence analysis of decellularized CRC biopsy before (TDM) and after repopulation with ZSGreen-labelled HT29 CRC cell line (TRM); Right panels, Scanning electron microscopy analysis of decellularized CRC biopsy before (TDM) and after repopulation with ZSGreen-labelled HT29 CRC cell line (TRM). Scale bar=10μm. D: Histology and immunohistochemistry staining of 3D-pCRC model: Hematoxylin and Eosin (H&E, upper panel), Periodic acid–Schiff (PAS, middle panel) and KI-67 marker of proliferation (lower panel). Scale bar=100μm. Directly from submitted paper: Reconstructed colorectal cancer model to dissect the anti-tumor effect of mesenchymal stromal cells derived extracellular vesicles – D'Angelo E. et al.

For the 3D-pCRC model, biopsies derived from primary tumor from high-risk stage II and III CRC patients were decellularized with different detergent-enzymatic treatment (DET) cycles, as previously demonstrated.[14] Tumor decellularized matrix (TDM) were repopulated by injection of HT29 cells. The recellularization protocol followed in the study was resumed in Figure 16B. Qualitative evaluation of HT29-recellularized samples were performed through histological and immunofluorescence analyses. In Figure 16C, the appearance of decellularized and HT29 re-cellularized matrices (TDM and TRM respectively) was evaluated. HT29 ZSgreen was able to colonize the tumor matrix and consistently distributed in almost all the areas of the decellularized tissue (Figure 16C, left panel). SEM analysis confirmed the ECM ultrastructure preservation after the decellularization and the presence of CRC cells within the re-cellularized matrix (Figure 16C, right panel). ECM components such as glycosaminoglycans and glycoproteins were uniformly distributed in the TRM, as observed by PAS staining (Figure 16D). H&E showed that HT29 cells were able to adhere, engraft and colonize the TDM. At 120 h after injection, we observed both spherical clusters at the edge and invasive spindle-shaped colon cancer cells migrating through the entire TRM (Figure 16D). Finally, the presence of Ki67-positive cells in the re-cellularized matrices confirmed that cells are actively proliferating after the TDM repopulation (Figure 16D). The results confirmed the possibility to use the 3D-pCRC as a model to study the role of MSC-derived EVs as therapeutics in the pathogenesis of CRC.

3.3.3 MSC-EVs EFFECT IN THE 3D-pCRC

Tumor 3D structures are strongly applied for drug testing in multiple tumor settings[95]. The diffusion capacity of MSC-EVs within the TDM and TRM has been explored. For this purpose, medium DiI-labelled-EVs (EVs-DiI) or control Dil-labelled PBS (PBS-DiI) were added to the TRM (Figure 17A). DiI-labelled-EVs were efficiently captured by the re-cellularized matrices as detected by the two-fold increase of the EV-selective fluorescence signal measured by fluorometer in the TRM after 120 h of treatment (Fig.17B). By confocal immunofluorescence analysis, the accumulation of MSC-EVs, mainly in the cytoplasm of the infiltrating HT29, were confirmed. Moreover, no DiI-positive signal was detected in HT29 that were incubated with the PBS-DiI, excluding the presence of residual unbounded DiI (Fig.17C). 3D reconstruction of decellularized matrices treated with MSC-EVs, showed that the particles were able to diffuse into TDM also in the absence of cancer cells with a homogenous pattern (Figure 17D, left side), supporting EVs capability to migrate inside the ECM interlaces. Interestingly, aggregates of several micrometers in size were observed embedded inside the ECM (Figure 17D, right side), suggesting a specific tropism of MSC-EVs for some components within the matrix. Furthermore, the effects of MSC-EVs on HT29 in the 3D-pCRC model were evaluated at the protein level as schematically represented in figure 18A. We hypothesized that MSC-EVs can affect cancer cell behavior directly, by their cellular uptake and/or indirectly, by modifying the biological and biochemical properties of patient-derived ECM. Moreover, the presence of

cancer cells in the TRM could directly modify the ECM structure and composition. Therefore, to discriminate the EVs activity, the proteomic profile of TDM and TRM were first compared.

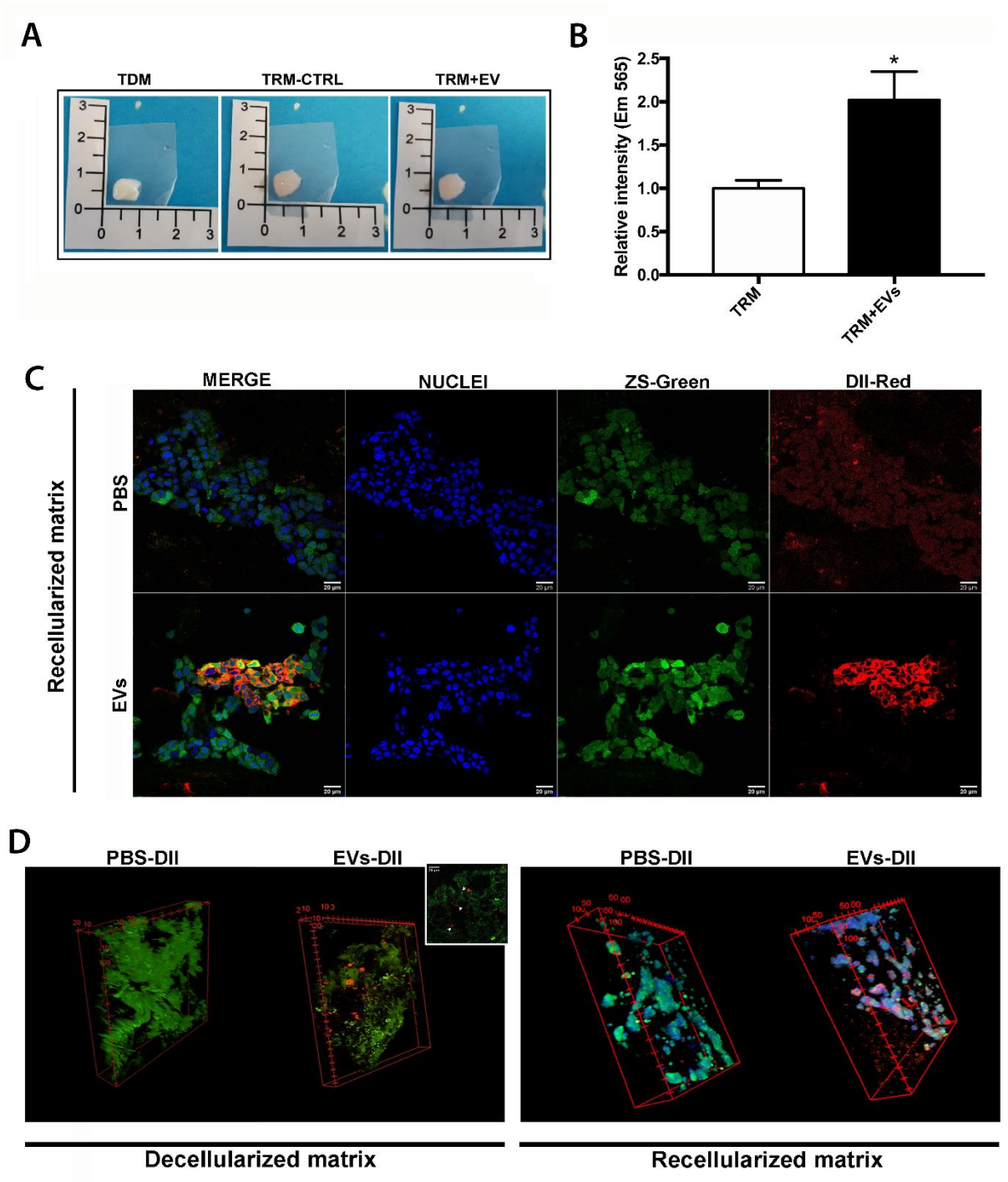

Figure 17 - MSC-EVs passive migration in decellularized CRC biopsies and active uptake in the 3D-pCRC model. A: Representative images of uniformly sized decellularized CRC biopsies (TDM), decellularized CRC biopsies repopulated with HT29 CRC cell line incubated with PBS-DiL (TRM-Ctrl) and decellularized CRC biopsies repopulated with HT29 CRC cell line incubated with EVs-DiL (TRM+EV). B: Quantification of DiL-associated fluorescence recorded at 565nm emission wavelength in decellularized CRC biopsies repopulated with HT29 CRC cell line incubated with PBS-DiL (TRM-Ctrl) and decellularized CRC biopsies repopulated with HT29 CRC cell line incubated with EVs-DiL (TRM+EV). C: Representative immunofluorescence images of decellularized CRC biopsies repopulated with ZSGreen-HT29 CRC cell line incubated with EVs-DiL or PBS-DiL. Cell nuclei were counterstained using DAPI. Scale bar=20µm. D: DiL-labelled MSC-EVs (red) diffusion in decellularized CRC biopsies (left panel) and decellularized CRC biopsies repopulated with ZSGreen-HT29 CRC cell line (green, right panel; scale bar = 20 µm). Directly from submitted paper: Reconstructed colorectal cancer model to dissect the anti-tumor effect of mesenchymal stromal cells derived extracellular vesicles – D'Angelo E. et al.

after incubation with MSC-EVs. TDM and TRM incubated with conventional growth media were used as control. As shown in Figure 18B, we identified a total of 110 differently expressed proteins between TRM EV and TDM EV, 107 were up-regulated and 3 were down-regulated in TRM EV compared to TDM EV (Figure 18B).

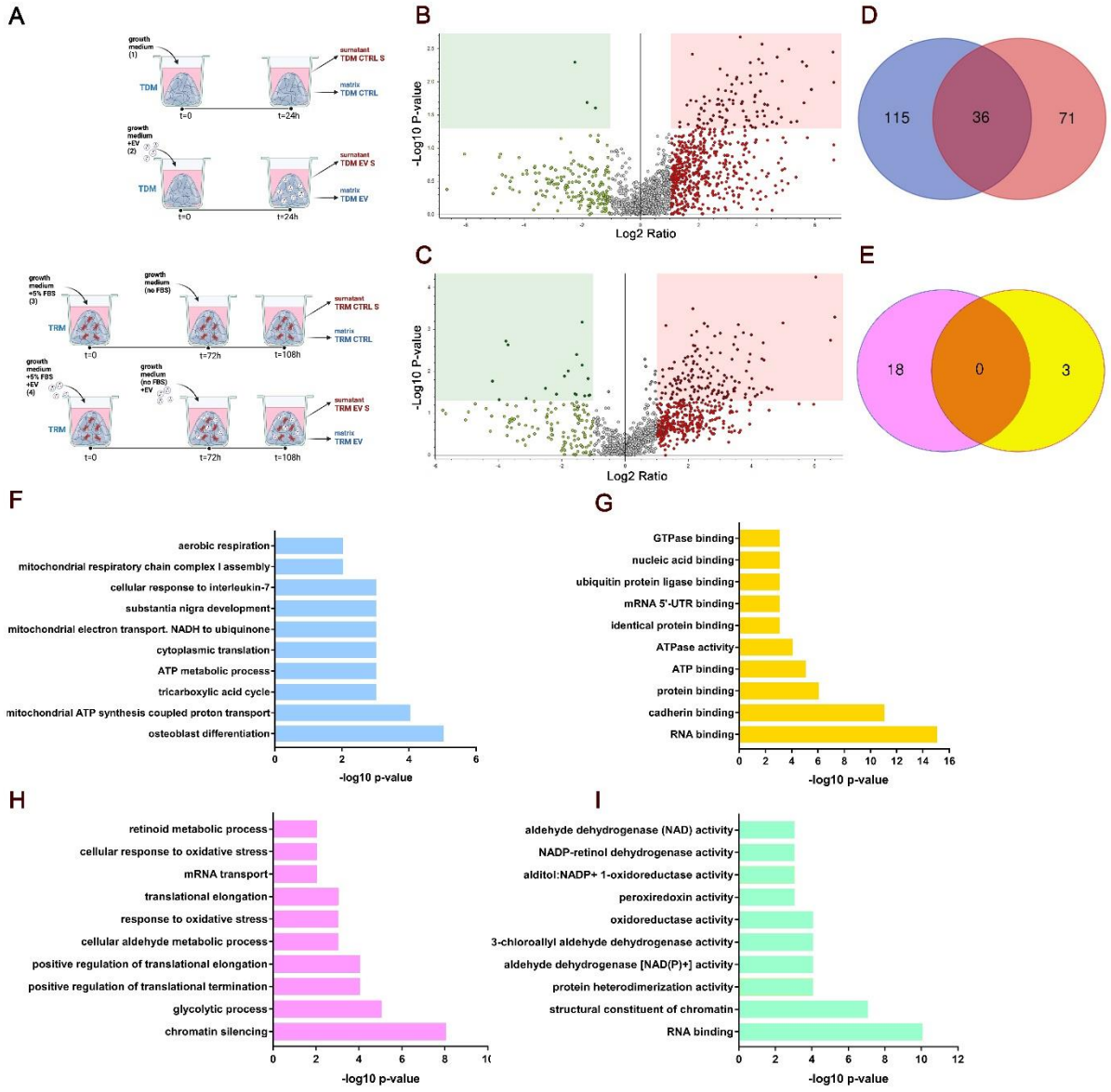

Figure 18 - Proteome analysis of TDM and TRM samples. A: Schematic representation of proteome and secretome analysis in TDM and TRM samples in which differentially abundant proteins were investigated in TDM (upper panel) or TRM (lower panel) after EV-treatment or not. Matrix samples were divided into four groups: (i) decellularized CRC biopsies, EV-untreated (TDM CTRL) or (ii) EV-treated (TDM EV); (iii) decellularized CRC biopsies repopulated with HT29 CRC cell line, EV-untreated (TRM CTRL) or (iv) decellularized CRC biopsies repopulated with HT29 CRC cell line EV-treated (TRM EV). B-C: Volcano plots of the comparison between the proteomic profile of TRM and TDM after incubation with MSC-EVs (B) or control cells growth medium (C); up-regulated proteins (red squares) and down-regulated proteins (green squares). D-E: Venn diagrams of up-regulated (D) and down-regulated (E) proteins in the proteomic profile comparison of TRM EV vs TDM EV and TRM CTRL vs TDM CTRL. Up-regulated proteins specific of CTRL group are labelled in blue, those specific of EVs treated-group are in red and the up-regulated proteins shared by the two groups are in dark red. Down-regulated proteins specific of CTRL group are labelled in pink, those specific of EVs treated-group are in yellow and the down-regulated proteins shared by the two groups are in orange. F-I: Functional annotation of the up-regulated proteins in TRM CTRL using DAVID Bioinformatics Resources, Biological processes (F) and Molecular functions (G). Functional annotation of the up-regulated

proteins in TRM EV using DAVID Bioinformatics Resources, Biological processes (H) and Molecular functions (I). Directly from submitted paper: Reconstructed colorectal cancer model to dissect the anti-tumor effect of mesenchymal stromal cells derived extracellular vesicles – D'Angelo E. et al.

In parallel, 170 differently expressed proteins were recognized between TRM CTRL and TDM CTRL (Figure 18C). Among these proteins, 152 were up-regulated and 18 were down-regulated TRM CTRL compared to TDM CTRL. Next, the two lists have been compared to discriminate the direct effects of MSC-EVs on the infiltrated colon cancer cells. Considering the up-regulated proteins, a total of 36 proteins were shared by the two groups, with the others 115 and 71 being exclusively modulated in CTRL or EV-treated groups, respectively (Figure 18D). In the case of down-regulated proteins, 18 were specific for CTRL and 3 for EV-treated groups with no shared molecules (Figure 18E). The 115 up-regulated proteins in TRM CTRL were functionally annotated using DAVID Bioinformatics Resources. Among the over-represented biological processes, we identified processes mainly involved in mitochondrial and ATP metabolic regulation (Figure 18F). This was related molecularly with active transcriptional mechanisms, ATPase and GTPase activity (Figure 18G). On the contrary, the functional annotation of the 71 up-regulated proteins in TRM EV showed a strong representation of biological processes related with transcriptional inhibition and oxidative stress response (Figure 18H). The most significant molecular functions were involved in metabolic activity and RNA binding mechanism (Figure 18I). Interestingly, among the most noteworthy molecular functions, we also identify four independent GO terms for different cell oxidoreductase pathways represented by a group of 16 proteins. In detail, oxidoreductase activity (GO:0016491), peroxiredoxin activity (GO:0051920), alditol: $NADP^+$ 1-oxidoreductase activity (GO:0004032) and oxidoreductase activity acting on the aldehyde or oxo group of donors NAD or NADP as acceptor (GO:0016620) (Figure 18I). Analyzing at the individual level the proteomic composition of EV-treated samples, we observed an enrichment for proteins involved in stress conditions and proliferation inhibition. Among them, calmodulin (CALM1) and 14-3-3 protein sigma (SFN) showed respectively a 47,2- and 41,7-fold change up-regulation in TRM EV compared with TDM EV. Conversely, EV-untreated samples showed an enrichment for proteins involved in the active state of cellular proliferation, such as prosaposin (PSAP) and stathmin (STMN1), which showed respectively a 25,2- and 20,2-fold change up-regulation in TRM CTRL compared with TDM CTRL. Then, the direct biological activity of MSC-EVs on the 3D-CRC model was evaluated. EVs derived from adult stem cells were previously demonstrated to mediate anti-tumor activity in different tumor cells. The repopulation capability of HT29 cancer cells repopulation capability was analyzed by assessing their proliferation and apoptosis into the decellularized ECM. The multiple administration of MSC-EVs (10K EVs/target cells) significantly reduced the number of HT29 invading the decellularized ECM as observed by H&E staining (Figure 19A). This reduction in the number of repopulating HT29 cells was accompanied by a significant increase in the number of apoptotic cells in MSC-EVs treated TRM in respect to TRM CTRL (24,88±4,4 vs 7,00±1,7/field, $p<0,01$) detected by TUNEL assay (Figure 19A-B). Moreover, we observed a significant downregulation of anti-apoptotic B-cell lymphoma 2 (BCL-2) transcript and the upregulation of Bcl-2 homologous antagonist/killer BAK1 gene thus confirming the TUNEL results (Figure 19C). MSC-EVs were also able to impair proliferation of HT29 cells inside the matrix as detected by the downregulation of the pro-proliferative genes MYC proto-oncogene

(c-MYC) and proliferation marker Ki-67 (KI-67), the Cyclin-D2 (CCND2) and -E1 (CCNE1) and the upregulation of the Cyclin Dependent Kinase Inhibitor 1A (CDKN1A) (Figure 19C).

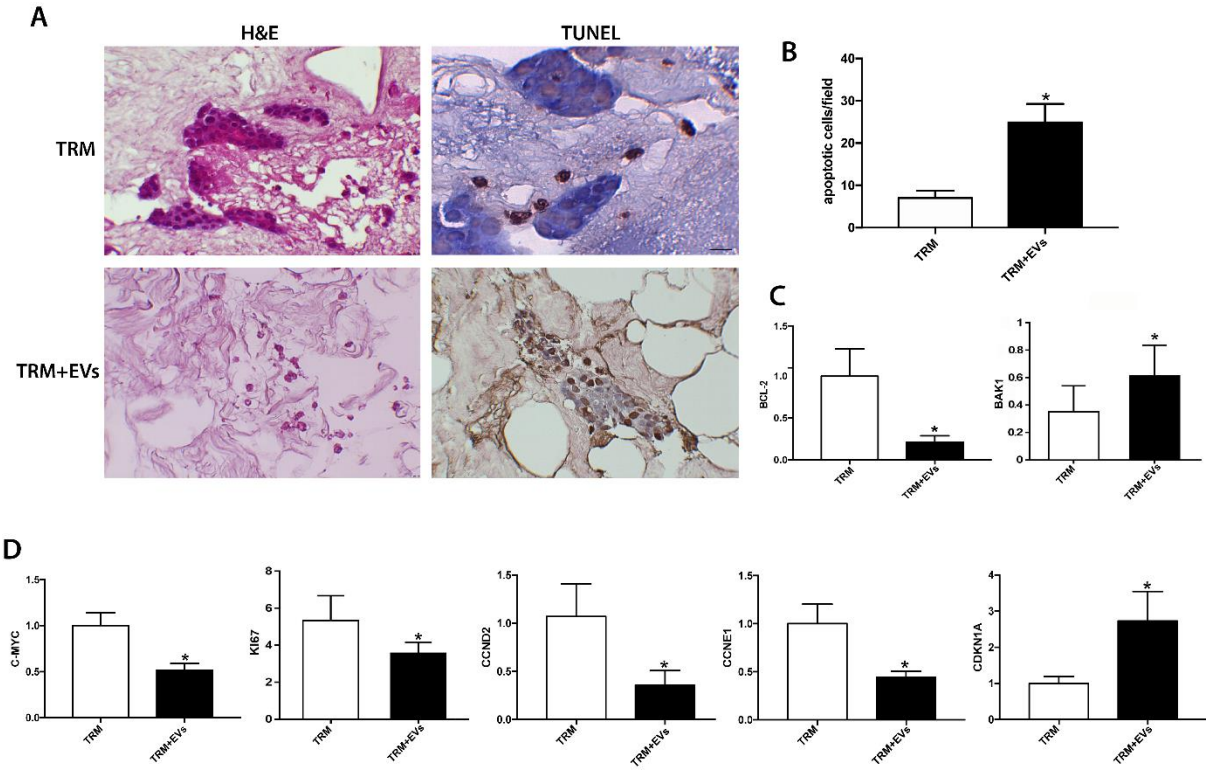

Figure 19 - Biological effect on cell cycle and apoptosis of the MSC-EVs treatment in the 3D-pCRC model. A: Representative images of 3D-pCRC treated or un-treated with MSC-EVs (left panel). The apoptotic cells were detected using TUNEL assay, the DNA fragmentation is indicated by ApopTag Plus Peroxidase positive staining (brown). Scale bar = 100 μm. B: Quantification of apoptotic cells in the 3D-pCRC model treated or un-treated with MSC-EVs. C-D: Gene expression level of cell cycle-related genes in the 3D-pCRC model treated or un-treated with MSC-EVs: (C) BCL-2 and BAK1. (D) C-MYC, KI-67, CCND2, CCNE1 and CDKN1A. Directly from submitted paper: Reconstructed colorectal cancer model to dissect the anti-tumor effect of mesenchymal stromal cells derived extracellular vesicles – D'Angelo E. et al.

Lastly, a secretome analysis of the proteins released by EV-treated matrices (TDM and TRM) was conducted to investigate the ECM changes induced by the treatment. In TDM samples, because of the extremely low abundance of secreted proteins, a qualitative comparative analysis was performed. A total of 1256 proteins were identified in the secreted profile of TDM EV and TDM CTRL; 465 of them were commonly shared among the two groups, while 403 and 388 were specific of the secreted profile of TDM CTRL and TDM EV, respectively (Figure 20A). The 403 TDM CTRL-specific secreted proteins were functionally annotated using DAVID Bioinformatics Resources. Among the over-represented biological processes, we identified processes mainly involved in mitochondrial metabolism and tricarboxylic acid cycle regulation. While the most significant molecular functions were related to actin and cytoskeletal remodeling and cell-cell and cell-ECM binding (Figure 20B-C). Similarly, the 388 TDM EV-specific secreted peptides were functionally annotated using DAVID Bioinformatics Resources. Among the over-represented biological processes, we identified processes mainly involved in epigenetic silencing of gene expression and nuclear organization of chromatin. While the most significant molecular functions were related to extracellular matrix structural constituent and ECM-remodeling enzymes (Figure 20D-E). In the HT29-repopulated samples,

we identified a total of 24 differently expressed proteins, of which 23 were up-regulated while 1 was down-regulated (Figure 20F). The GO biological processes

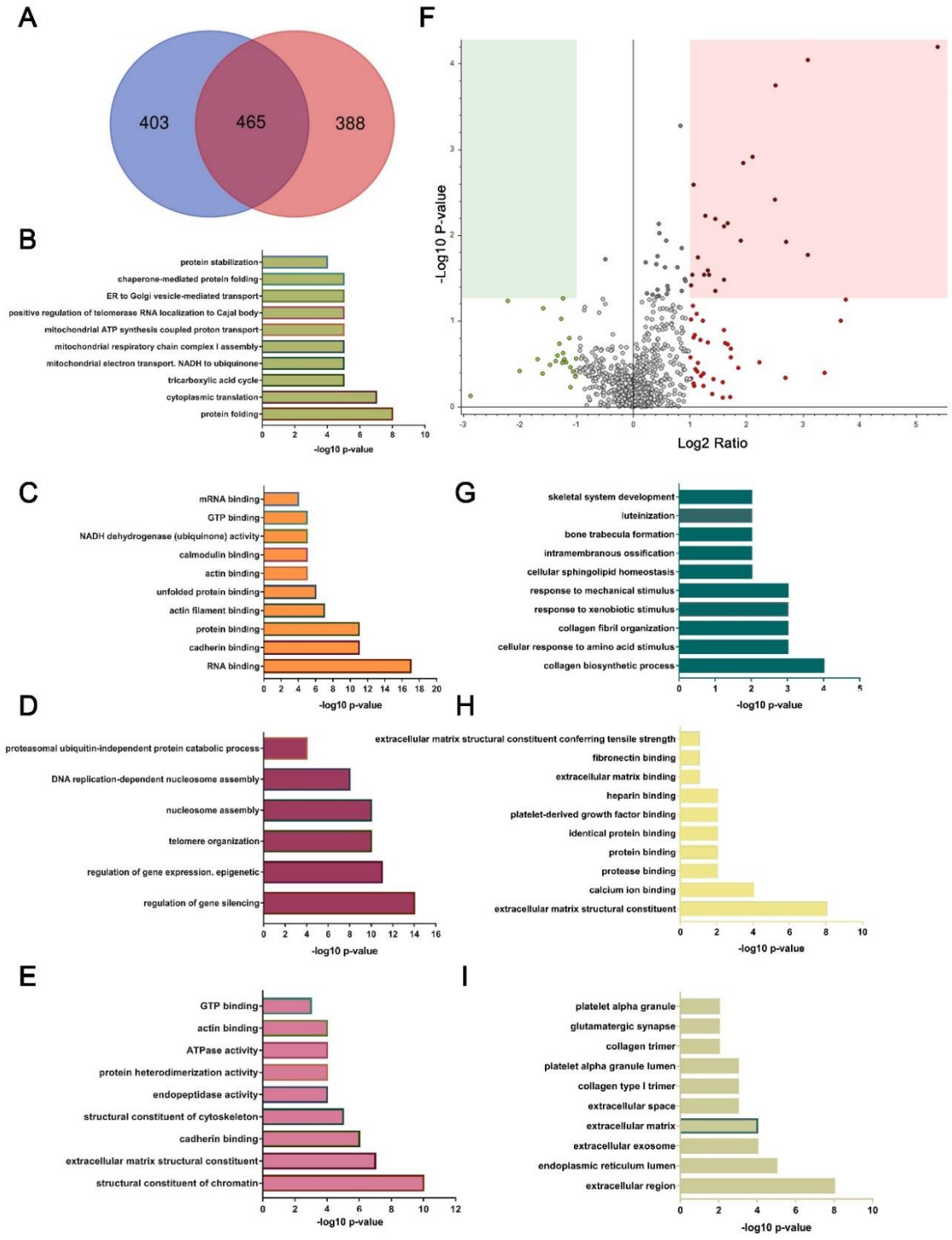

Figure 20 - Secretome analysis of TDM and TRM samples. (A) Veen diagram of identified protein specific of TDM EV (red), specific of TDM CTRL (blue) and in common (dark red). The 403 TDM CTRL-specific secreted proteins were functionally annotated using DAVID Bioinformatics Resources in (B) Biological processes and (C) Molecular functions. The 388 TDM EV-specific secreted proteins were functionally annotated using DAVID Bioinformatics Resources in (D) Biological processes and (E) Molecular functions. (F) Volcano plots of the comparison between the secretome profile of TRM-EV vs TRM CTRL, up-regulated proteins in TRM EV compared to TRM CTRL (red squares) and down-regulated proteins (green squares). The 23 secreted proteins up regulated in TRM EV were functionally annotated using DAVID Bioinformatics Resources in (G) Biological processes, (H) Molecular functions and (I) Cellular components. Directly from submitted paper: Reconstructed

overrepresented by the 23 up-regulated proteins were strongly associated with collagen biosynthesis and organization (Figure 20G). Among the molecular functions the most represented were related to ECM structural constituents and their binding (Figure 20H), associated with the extracellular exosome and matrix cellular components (Figure 20I). Interestingly among the most over-expressed proteins, we identified some secreted proteins related to ECM organization and remodeling and cell shape modification: secreted protein acidic and rich in cysteine (SPARC), calumenin (CALU), reticulon-4 (RTN4) and reticulocalbin-3 (RCN3) showed respectively a 3,1-; 2,5-; 2,5- and 2,4- positive fold change in TRM EV compared with TRM CTRL. Conversely, the only down-regulated protein was the adenylated kinase 2 (AK2), showing respectively a 0.4-fold change reduction in TRM EV compared with TRM CTRL.

CHAPTER 4: DISCUSSION

4.1 EVs IN CRC MICROENVIRONMENT

The present study describes for the first time a general picture of EVs in the contest of CRC microenvironment. We characterize for the first time the EV profile within ECM in cancer and surrounding mucosa, using decellularized tissues. Several studies in the literature suggest that the tumor microenvironment, characterized by hypoxia, starvation, and acidosis, promotes the release of extracellular vesicles into the tumor microenvironment, thereby enhancing carcinogenesis.[89–91,96] The ECM, the main non-cellular component of TME, is now considered an important reservoir of EVs, that modulates their functions and activity, regulating their stability and destination. In the tumor context, tissue derived EVs have been isolated either from fresh tissues, including colon carcinoma[97], leading to the recovery of the EVs present in the different tissue compartments, such as interstitial fluids, matrix and blood or directly derived from cells. Alternatively, EVs have been isolated by cultured tissues (for instance mouse melanoma[98], and human renal carcinoma.[99] We here selectively focused on TISSUE-EVs and ECM EVs, analyzing fresh and decellularized colon carcinomas and adjacent non-tumoral mucosa, to get insights on the possible role of TISSUE-EVs and ECM-EVs entrapped in the TME and their effect on adjacent tissues modification. Indeed, previous reports indicate that the tumor matrix is modified according to tumor malignancy and by itself may drive tumor progression.[98] Moreover, we assessed the surface markers profile representative of different cell populations possibly present within the cell microenvironment, the ECM or derived from circulation. Results on TISSUE-EVs confirmed an increased release of CRC-TISSUE-EVs in comparison with HC-TISSUE-EVs. This data differs from the one obtained in ECM-EVs suggesting that TME alteration are influencing EVs trapping within the ECM in a unique way. Several reports indicate that EV cargo influences the tumor microenvironment by activating molecular pathways that differ, in part, from the ones modulated by soluble factors.[23] Tumor angiogenesis, invasion, and immune escape are highly modulated by EVs and play a relevant role in tumor progression.[14,16] In addition, EVs may promote the development of the pre-metastatic niche, infiltrating normal tissue and favoring microenvironment alteration such as angiogenesis and immune tolerance.[4] We observed that surface marker analyses on TISSUE-EVs mirrored the alteration already described in the cell TME. CRC-TISSUE-EVs showed an increased expression of platelet marker (CD42a, CD62p and CD142), myeloid markers (CD11c, CD14 and HLA-DR) and lymphoid marker (CD24, CD25, CD40 and CD86), except for NK marker (CD56). It has been previously observed that platelet count and activation levels are significantly higher in tumor tissue compared to healthy tissue. CD42a (GPIX), along with other platelet markers, forms a complex that serves as a receptor for von Willebrand factor, which mediates platelet activation. Activated platelets release alpha granules, which in turn secrete TGF-β, VEGF, and PDGF. These factors not only induce tumor growth, but also promote angiogenesis and tumor neovascularization.[100] Interestingly, also the angiogenetic marker CD31 was found to be increased on CRC-TISSUE-EVs. In general, angiogenesis is a fundamental process in tumour growth and metastasis, as reported extensively in the literature. The formation of new blood vessels is essential for the delivery of nutrients and oxygen to the tumour and inhibition of angiogenesis has been considered as a potential therapeutic strategy

for cancer treatment. Also, CD142 (TF, coagulation factor III), the main physiological initiator of normal blood coagulation, is expressed on the surface of multiple cancer cells,[101] and our analysis confirmed its higher expression in tumor tissue derived EVs than in healthy tissue derived EVs. Moreover, tumor cells that enter the bloodstream during the metastatic process are exposed to high stress and to the immune system. To survive, tumor cells can bind to activated platelet that express P-selectin (CD62p) through tumor cell-induced platelet aggregation (TCIPA) and form aggregates to protect themselves from the bloodstream and "hide" from natural killer (NK) cells.[102] The CD56 reduction observed in our study also reflects the “behavior” of cancer cells to evade the immune system for growing and metastasized. In fact, NK cells can recognize and killing cancer cells, release cytokines and chemokines that regulate the immune system. For this reason, are frequently reduced in tumor as immune escape mechanism.[103] In our analysis, the values of CD11c and CD14, markers expressed on dendritic cells, were found to be significantly higher in the tumor than in healthy tissue. Dendritic cells play a controversial role in various tumors, including CRC, according to previous studies. On the one hand, since they are antigen-presenting cells, they are responsible for maintaining local immunity and recruiting anti-tumor T cells. On the other hand, it has also been seen that there are dendritic cells with immunosuppressive activity that can be recruited to tumors, causing T cell tolerance and progressive tumor growth.[104] Also HLA-DR, a class II antigen presentation molecule, was found to be higher in the CRC-TISSUE-EVs compared to HC-TISSUE-EVs. HLA-DR is normally expressed on antigen-presenting cells including monocytes, macrophages, and dendritic cells, but in general, myeloid expression can be induced on tumor cells in response to inflammatory conditions.[105] Contrary, HLA-ABC, a class I antigen presentation molecule, was found to be higher in healthy tissue than in the tumor. In previous studies, the expression of HLA-ABC was analyzed in breast cancer, and it was demonstrated that a deficiency in class I HLA molecules may lead to a down-regulation of T cell-based immune surveillance, which can ultimately result in tumor development and progression. Based on our study on colon rectal cancer, it can be hypothesized that CRC-EVs may have a similar effect by altering the HLA expression and contributing to immune evasion.[106] Also tissue specific markers (CD29, CD44, CD146) were found to be increased in HC-TISSUE-EVs suggesting a tissue-phenotype loss in tumor tissue. Furthermore, Dan Liu and colleagues reported that CD146 suppresses cancer stemness and CRC tumorigenesis by inactivating the Wnt/β-catenin signaling pathway. CD146 suppresses stem cell properties and epithelial phenotypes in CRC cells (increased expression of EpCAM and E-cadherin).[107] According with this study, in our analysis, CD146 was found to be significantly higher in healthy tissue than in the tumor. It could thus be hypothesized that the reduction of CD146 in tumor cells could induce the dedifferentiation of CRC cells and promote tumor growth. By carrying molecules that reflect the surface markers of the parent cell, EVs can be a valuable resource in liquid biopsy, which involves non-invasive collection of biological samples from bodily fluids such as blood or urine. EV analysis can provide useful information on the presence and spread of tumors, as well as their response to therapeutic treatments. For this reason, EVs are increasingly attracting attention as potential biomarkers for cancer monitoring and the development of personalized therapies[108] The markers that were presenting the best sensitivity and specificity on ROC curves were four: CD42a, CD44, CD56 and CD146. These markers have attracted particular interest as they provide information on the characteristics of TME present in the

analyzed tissue. In particular, CD146 has been associated with the suppression of tumor stemness and CRC tumorigenesis through inactivation of the Wnt/β-catenin signaling pathway. CD44 has been associated with the epithelial phenotype, CD42a has been associated with platelet activation and CD56 has been linked to immune escape mechanisms. The combined analysis of these markers can provide a more comprehensive view of the tumor condition, which could be useful for the development of new diagnostic and therapeutic strategies. Furthermore, we supported the increased tumor invasiveness of CRC-TISSUE-EVs in comparison to vesicles extracted from healthy colon mucosa. Results on non-cellular TME highlighted a significant modification in the HC-ECM surrounding the primary cancer lesions in the stage IV cancer with increase in EVs expressing immune and platelet markers. In addition, we identified, as previously described for CRC-TISSUE-EVs, CD25 as a marker specifically and selectively overexpressed in CRC-ECM-EVs of stage IV tumor tissue in respect to lower tumor stage and HC-ECM-EVs. We here found that ECM-EVs in tumor tissue mainly expressed immune and platelet markers, together with epithelial cell markers, indicating an abundance of circulating cell-derived EVs within the ECM. It is conceivable that these ECM-EVs could possibly originate from tissue infiltrating cells, but it cannot be excluded that blood- or lymph-derived EVs may directly extravasate. Interestingly, in our study, the EV profile in ECM of colonic primary tumor and healthy mucosa was specifically different only in patients with stage IV colon tumor. We here report a specific profile, characteristic of the stage IV tumor surrounding mucosa, with increase in markers of endothelium, such as CD105 and CD62p, and of platelets such as CD42a and CD49e. The presence of platelet-derived EVs within ECM is indeed of great interest, as tumor-educated platelets are considered an important player in cancer progression and metastasis.[102] These results suggest that both TISSUE- and ECM-EV are actively involved in creating a supportive microenvironment for tumor progression and for its infiltration in the surrounding tissues. Moreover, many evidences support that the immunological data could better predict patient survival than the histopathological methods in CRC.[109–111] However, only few data recently demonstrated that immune microenvironment content in the healthy mucosa of gastrointestinal tract might provide a picture of the local immune response to cancer thus giving further information on cancer progression and on the recurrence risk when cancer tissue is no more available.[112] Intriguingly, in this line, we demonstrated that ECM-EVs isolated from peritumoral healthy mucosa differ between stage II-III CRC compared to stage IV CRC with platelet and inflammatory cell infiltration, and possibly activation of epithelial cells. These data, once more, suggest how the immune status and relative EVs profile on the healthy peri-tumoral colon mucosa is related to the tumor stage and could be an interesting field of study as surrogate prognostic biomarker after curative surgery in CRC. Finally, another relevant finding of our study is the identification of EVs carrying CD25 specifically and selectively in cancer tissue and in stage IV tumor ECM in respect to lower tumor stage. CD25, a component of the IL-2 receptor, is important in T cell proliferation, and expressed by both regulatory and effector T cells.[113,114] Although we cannot ascribe the CD25 expressing CRC-EVs to one of this population, CD4+CD25+Foxp3+ T regulatory cells are known to be increased both peripherally and at the tumor site in a multitude of human cancers, including colon cancer[115,116], suggesting that CD25-ECM-EVs may rather derive from T regulatory cells.

4.2 DECELLULARIZED ECM AS A 3D-pCRC

To explore the use of EVs as a therapeutic strategy, in this study we also evaluate the MSC-EVs effect on CRC. Today, it is well established that MSCs can regulate tumor cell fate mostly in a paracrine manner rather than in a cellular mediated action. In this context, a major contribution as paracrine effector was proposed to the MSC-released EVs.[117] MSC-EVs has been described to modulate tumorigenesis thanks to their tropism toward tumor sites and their capacity to vehiculate bioactive molecules and drugs.[118] However, data about the exact role(s) played by MSC-derived EVs on cancer biology are still conflicting. In this landscape, even more limited evidence is available on the EV trafficking and uptake in 3D in vitro models where the simultaneous presence of cancer cell and patient-derived ECM can affect the EVs function.[95] Here, we demonstrated through the use of a 3D-pCRC model that: a) MSC-EVs are capable to diffuse through tumor ECM and be up taken by ECM-engrafted colon cancer cells; b) MSC-EVs treatment of HT-29 have an anti-tumor effect of halting cell proliferation affecting cell cycle proteins; c) Extracellular matrix organization, cell cycle metabolism and epigenetic regulation of transcription, are the biological processes primarily deregulated by the MSC-EVs administration in the 3D-pCRC.We first isolated and characterized EVs from MSCs to be used in our assay. The positivity for classical MSC-EV markers was confirmed (i.e. CD29, CD44, CD146, CD49e, CD105, HLA-ABC, CD9, CD63 and CD81)[93] To get better insight in the characterization of MSC-EVs, we examined their protein cargo. The molecular pathways highlighted by our identified MSC-EV proteins were mainly involved in DNA synthesis and transcription, telomer organization, epigenetic gene silencing and ECM organization. On one hand, the finding of proteins involved in DNA synthesis/regulation fits with our hypothesis that EVs can regulate cell cycle of tumor cells at distinct levels. On the other hand, the presence of proteins involved in ECM organization supports the recent insights on EVs function as ECM remodeling effectors to promote/control cancer progression and dissemination[119–123]. Interestingly, we identified molecules belonging to the complement system as a highly representative protein family in MSC-EVs cargo. The complement system activation, in the oncological context, has been considered as part of the body's immunosurveillance mechanisms against cancer.[124] However, it is to note that in both physiological and pathological contexts complement molecules are inactive and must be activated by specific trigger signals. Among these triggers, the long-pentraxin PTX3, functions as antibody mimic and activates/regulates the classic pathway of complement initiation.[125] PTX3 was detected in the EV cargo as well as in both EV-treated decellularized and re-cellularized matrices but was absent in the untreated counterparts, these data support the possible role of PTX3 as a trigger of complement canonical pathway activation[126] supporting the anti-tumor effect of MSC-EVs on CRC cells. A clear association between PTX3 deficiency and an increased susceptibility to mesenchymal and epithelial carcinogenesis was observed in different tumors including CRC[127]. The potential use of MSC-EVs as a bioactive compound with per se anti-tumor activity is dependent from their internalization capability into a three-dimensional complex tumor microenvironment, Interestingly, EVs can diffuse through the porous mesh of our patient-derived colon cancer matrix. In particular, the detection of EVs not only at the edges of patient-derived ECM but also in its inner core region may suggest the presence of a matrix-dependent mechanism of EV transportation. Our results are in line with and support those recently published by Lenzini et al., which demonstrated that EVs can modify their shape and escape the ECM-derived hydrogel

structure by finely changing the function of water-transporting aquaporins[25]. To understand the complex interaction of MSC-derived EVs with the tumor and the ECM components, we dissected the proteome profiles of cancer cells exposed to MSC-EVs in the 3D-pCRC model. An enrichment of proteins related to gene silencing, negative regulation of translational processes and oxidative stress was identified in MSC-EVs treated matrix, outlining the picture of a cell population exposed to stress conditions and a negative regulation of cell growth. Among the modulated proteins, Calmodulin 1 (CALM1) was specifically up-regulated in TRM-EVs compared to TDM-EVs. CALM1 can interact with 14-3-3 and various cyclin-dependent kinases by controlling the G1/S to G2/M transition, via the regulation of Ca2+ intracellular concentration.[128] Conversely, control repopulated matrix showed an enrichment for proteins involved in biological processes typical of cells in an active state of proliferation. Among them, Prosaposin (PSAP) a glycoprotein promoting cancer proliferation and tumorigenesis and over-expressed in multiple solid tumours[129], as well as Stathmin (STMN1), a microtubule-regulating protein, whose upregulation was directly correlated with cell migration in solid tumor.[130] This led us to speculate that colon cancer cells exposed to MSC-EVs, when cultivated in patient-derived ECM, could experience a reduction in cell plasticity preventing cell homing and migration in the tumor matrix scaffold. This was confirmed by a clear reduction in the number of CRC cells detected in the matrix after MSC-EVs administration. Finally, we demonstrated a strong decrease of viability of EV-treated CRC cells, due to an enhanced apoptosis occurred in HT-29, as evidenced by Tunel assay. At transcript level, the downregulation of pro-proliferative molecules such as Ki-67 and c-Myc and the cyclins, CCND2 and CCNE1, in concomitant with the over-expression of CDKN1A, negative regulator of G1/S transition, confirmed a molecular fingerprint associated with the block of cell cycle induced by the EV treatment.[131,132] The secretive profile of EV-treated TRM was consistent with the proteomics data obtained in the 3D-CRC model, showing an enrichment of proteins related to calcium ion binding and an ECM organization with respect to the untreated TRM. These data support a dual role of MSC-EVs in targeting (i) the cellular mechanisms that regulate the balance between cell proliferation and cell death and (ii) the peri-cellular structural microenvironment, controlling cancer cell adhesion and migration. In line, we identified a cluster of proteins involved in the inhibition of migration/invasion (i.e. SPARC, CALU, RCN3 and RTN4), that resulted in being up-regulated in the secretome of repopulated matrices treated with MSC-EVs compared to the untreated ones. SPARC, is a secreted protein member of a family of matricellular proteins, whose function is to negatively modulate cell–matrix interactions.[133,134] In addition, in colorectal cancer and other tumors (i.e. ovarian and neuroblastomas), it may function as tumor suppressor by inhibiting G1/S phase transition.[135,136] Interestingly CALU, RCN3 and 4 are high-molecular weight glycoproteins involved in fibrillar network formation, that efficiently inhibit cell migration and tumor metastasis.[137] Only one protein, AK2, resulted down-regulated in the EV-treated TRM compared to the untreated TRM. AK protein family members are key enzymes for the maintenance of the adenine nucleotide metabolic homeostasis, cell cycle regulation and ATP energy distribution[138], showing a pivotal role in tumor development.[139,140] Its decrease in abundance in the secretome of TRM EVs may thus indicate a possible regulation by MSC-EVs of cancer cell metabolism. For instance, Hansel et al. demonstrated that AK2 can be upregulated and promote nucleotide signal transduction and metastasis formation in pancreatic cancer. [141]

4.3 STUDY LIMITATIONS AND FUTURE PROSPECTIVES

The present study offers a promising area of investigation as a potential source of biomarkers for the diagnosis of colorectal cancer as well as a new 3D cancer model directly derived from patients. However, some limitations were pointed out. First, the panel of markers used to characterize EVs' surface markers is mainly related to blood-circulating EV markers. This allowed the profiling of microenvironments, and blood infiltrating cell derived EVs within the different component of TME but excluded other important tumor and microenvironmental components. Moreover, the MACSPlex kit provided a semiquantitative analysis of EV markers, and their confirmation and possible co-expression at a single EV level would be important. Moving on to 3D model, assessing viability and cytotoxicity of 3D-pCRC can be difficult using standard biochemical assays because of incomplete probe penetration and limited sensitivity. Furthermore, confocal microscopy, immunofluorescence, and electron microscopic techniques are useful for assessing morphology and internal organization, but these imaging techniques are challenging due to poor light penetration, light scattering by cells, and high background.

We can conclude that the analysis of EVs entrapped in the ECM of normal and tumor colon mucosa may provide information on the non-cellular microenvironment and its modulation during tumor progression and highlight a change in healthy mucosa ECM adjacent to high stage tumors of possible relevance for tumor spread. Differently, TISSUE-EVs reflect the molecular profile of cancer cells and how they manipulate the TME, thus providing an attractive option for the early detection and monitoring of tumour progression. However, it's needed additional research to establish their effectiveness and determine the most effective diagnostic and therapeutic strategies for utilizing these EVs in clinical practice. Moreover, we establish a promising assay to investigate the biological activity of MSC-EVs on colon cancer cells, in a 3D cancer environment. In the 3D-pCRC model, the direct influence of each biological component of the other (EVs, cancer and tumor-ECM) was discerned, allowing a better definition of the tumor-stroma response to EVs treatment. In the future, this 3D patient-derived model can be translated to other cancer models and EVs sources (naïve or engineered) to evaluate different anti-cancer drugs in a 3D biomimicking environment.

CHAPTER 5: BIBLIOGRAPHY

1. Théry, C. *et al.* Minimal information for studies of extracellular vesicles 2018 (MISEV2018): a position statement of the International Society for Extracellular Vesicles and update of the MISEV2014 guidelines. *J Extracell Vesicles* **7**, (2018).
2. Abbott A. FedEx for your cells: this biological delivery service could treat disease. Nature. 2023;621(7979):462-464. doi:10.1038/d41586-023-02906-w
3. Yáñez-Mó, M. *et al.* Biological properties of extracellular vesicles and their physiological functions. *J Extracell Vesicles* **4**, 1–60 (2015).
4. Ciardiello, C. *et al.* Focus on Extracellular Vesicles : New Frontiers of Cell-to-Cell Communication in Cancer. 1–17 (2016) doi:10.3390/ijms17020175.
5. Keum, N. N. & Giovannucci, E. Global burden of colorectal cancer: emerging trends, risk factors and prevention strategies. *Nature Reviews Gastroenterology and Hepatology* vol. 16 713–732 Preprint at https://doi.org/10.1038/s41575-019-0189-8 (2019).
6. Bray, F. *et al.* Global cancer statistics 2018: GLOBOCAN estimates of incidence and mortality worldwide for 36 cancers in 185 countries. *CA Cancer J Clin* **68**, 394–424 (2018).
7. Morgan E, Arnold M, Gini A, et al. Global burden of colorectal cancer in 2020 and 2040: incidence and mortality estimates from GLOBOCAN. Gut. 2023;72(2):338-344. doi:10.1136/gutjnl-2022-327736
8. Jasperson, K. W., Tuohy, T. M., Neklason, D. W. & Burt, R. W. Hereditary and Familial Colon Cancer. *Gastroenterology* **138**, 2044–2058 (2010).
9. Sagaert, X., Vanstapel, A. & Verbeek, S. Tumor Heterogeneity in Colorectal Cancer: What Do We Know So Far? *Pathobiology* **85**, 72–84 (2018).
10. Chen, K., Collins, G., Wang, H. & Toh, J. W. T. Pathological features and prognostication in colorectal cancer. *Current Oncology* **28**, 5356–5383 (2021).
11. Goiffon, R. J., O'Shea, A. & Harisinghani, M. G. Advances in radiological staging of colorectal cancer. *Clinical Radiology* vol. 76 879–888 Preprint at https://doi.org/10.1016/j.crad.2021.06.005 (2021).
12. Herzig, D. *et al.* The American Society of Colon and Rectal Surgeons Clinical Practice Guidelines for the Management of Inherited Polyposis Syndromes. *Dis Colon Rectum* **60**, 881–894 (2017).
13. Locker, G. Y. *et al.* ASCO 2006 update of recommendations for the use of tumor markers in gastrointestinal cancer. *Journal of Clinical Oncology* vol. 24 5313–5327 Preprint at https://doi.org/10.1200/JCO.2006.08.2644 (2006).
14. Piccoli, M. *et al.* Decellularized colorectal cancer matrix as bioactive microenvironment for in vitro 3D cancer research. *J Cell Physiol* **233**, 5937–5948 (2018).

15. Cirri, P. & Chiarugi, P. Cancer associated fibroblasts: the dark side of the coin. *Am J Cancer Res* **1**, 482–497 (2011).

16. Gabrilovich, D. I., Ostrand-Rosenberg, S. & Bronte, V. Coordinated regulation of myeloid cells by tumours. *Nat Rev Immunol* **12**, 253–268 (2012).

17. Cheng, L. *et al.* Glioblastoma stem cells generate vascular pericytes to support vessel function and tumor growth. *Cell* **153**, 139–152 (2013).

18. Anderson, N. M. & Simon, M. C. The tumor microenvironment. *Current Biology* vol. 30 R921–R925 Preprint at https://doi.org/10.1016/j.cub.2020.06.081 (2020).

19. Hanahan, D. & Weinberg, R. A. Hallmarks of cancer: The next generation. *Cell* vol. 144 646–674 Preprint at https://doi.org/10.1016/j.cell.2011.02.013 (2011).

20. Hanahan, D. & Folkman, J. *Patterns and Emerging Mechanisms Review of the Angiogenic Switch during Tumorigenesis*. *Cell* vol. 86 (1996).

21. Arneth, B. Tumor microenvironment. *Medicina (Lithuania)* vol. 56 Preprint at https://doi.org/10.3390/medicina56010015 (2020).

22. Friend, C. *et al.* Observations on cell lines derived from a patient with Hodgkin's disease. *Cancer Res* **38**, 2581–2591 (1978).

23. Webber, J. P. *et al.* Differentiation of tumour-promoting stromal myofibroblasts by cancer exosomes. *Oncogene* **34**, 290–302 (2015).

24. Cavallari, C., Camussi, G. & Brizzi, M. F. Extracellular vesicles in the tumour microenvironment: Eclectic supervisors. *International Journal of Molecular Sciences* vol. 21 1–21 Preprint at https://doi.org/10.3390/ijms21186768 (2020).

25. Lenzini, S., Bargi, R., Chung, G. & Shin, J. Matrix mechanics and water permeation regulate extracellular vesicle transport. *Nat Nanotechnol* **15**, (2020).

26. Huleihel, L. *et al.* Matrix-bound nanovesicles within ECM bioscaffolds. *Sci Adv* **2**, (2016).

27. Tao, S. C. & Guo, S. C. Role of extracellular vesicles in tumour microenvironment. *Cell Communication and Signaling* vol. 18 Preprint at https://doi.org/10.1186/s12964-020-00643-5 (2020).

28. Kalluri, R. The biology and function of exosomes in cancer. *Journal of Clinical Investigation* vol. 126 1208–1215 Preprint at https://doi.org/10.1172/JCI81135 (2016).

29. Sarhadi, V. K., Daddali, R. & Seppänen-Kaijansinkko, R. Mesenchymal stem cells and extracellular vesicles in osteosarcoma pathogenesis and therapy. *International Journal of Molecular Sciences* vol. 22 Preprint at https://doi.org/10.3390/ijms222011035 (2021).

30. Phinney, D. G. & Pittenger, M. F. Concise Review: MSC-Derived Exosomes for Cell-Free Therapy. *Stem Cells* **35**, 851–858 (2017).

31. Whiteside, T. L. Exosome and mesenchymal stem cell cross-talk in the tumor microenvironment. *Seminars in Immunology* vol. 35 69–79 Preprint at https://doi.org/10.1016/j.smim.2017.12.003 (2018).

32. Ridge, S. M., Sullivan, F. J. & Glynn, S. A. Mesenchymal stem cells: Key players in cancer progression. *Molecular Cancer* vol. 16 Preprint at https://doi.org/10.1186/s12943-017-0597-8 (2017).

33. Nicodemou, A., Bernátová, S., Čeháková, M. & Danišovič, Ľ. Emerging Roles of Mesenchymal Stem/Stromal-Cell-Derived Extracellular Vesicles in Cancer Therapy. *Pharmaceutics* vol. 15 Preprint at https://doi.org/10.3390/pharmaceutics15051453 (2023).

34. Mognetti, B., Montagna, G. La, Perrelli, M. G., Pagliaro, P. & Penna, C. Bone marrow mesenchymal stem cells increase motility of prostate cancer cells via production of stromal cell-derived factor-1α. *J Cell Mol Med* **17**, 287–292 (2013).

35. Quante, M. *et al.* Bone Marrow-Derived Myofibroblasts Contribute to the Mesenchymal Stem Cell Niche and Promote Tumor Growth. *Cancer Cell* **19**, 257–272 (2011).

36. Hmadcha, A., Martin-Montalvo, A., Gauthier, B. R., Soria, B. & Capilla-Gonzalez, V. Therapeutic Potential of Mesenchymal Stem Cells for Cancer Therapy. *Frontiers in Bioengineering and Biotechnology* vol. 8 Preprint at https://doi.org/10.3389/fbioe.2020.00043 (2020).

37. Liang, W. *et al.* Mesenchymal stem cells as a double-edged sword in tumor growth: focusing on MSC-derived cytokines. *Cellular and Molecular Biology Letters* vol. 26 Preprint at https://doi.org/10.1186/s11658-020-00246-5 (2021).

38. Timaner, M., Tsai, K. K. & Shaked, Y. The multifaceted role of mesenchymal stem cells in cancer. *Seminars in Cancer Biology* vol. 60 225–237 Preprint at https://doi.org/10.1016/j.semcancer.2019.06.003 (2020).

39. Caplan, H. *et al.* Mesenchymal Stromal Cell Therapeutic Delivery: Translational Challenges to Clinical Application. *Frontiers in immunology* vol. 10 1645 Preprint at https://doi.org/10.3389/fimmu.2019.01645 (2019).

40. Vizoso, F. J., Eiro, N., Cid, S., Schneider, J. & Perez-Fernandez, R. Mesenchymal stem cell secretome: Toward cell-free therapeutic strategies in regenerative medicine. *International Journal of Molecular Sciences* vol. 18 Preprint at https://doi.org/10.3390/ijms18091852 (2017).

41. Keshtkar, S., Azarpira, N. & Ghahremani, M. H. Mesenchymal stem cell-derived extracellular vesicles: Novel frontiers in regenerative medicine. *Stem Cell Research and Therapy* vol. 9 Preprint at https://doi.org/10.1186/s13287-018-0791-7 (2018).

42. Herrmann, I. K., Wood, M. J. A. & Fuhrmann, G. Extracellular vesicles as a next-generation drug delivery platform. *Nature Nanotechnology* vol. 16 748–759 Preprint at https://doi.org/10.1038/s41565-021-00931-2 (2021).

43. Dalmizrak, A. & Dalmizrak, O. Mesenchymal stem cell-derived exosomes as new tools for delivery of miRNAs in the treatment of cancer. *Frontiers in Bioengineering and Biotechnology* vol. 10 Preprint at https://doi.org/10.3389/fbioe.2022.956563 (2022).

44. Zhang, S. *et al.* MSC exosomes mediate cartilage repair by enhancing proliferation, attenuating apoptosis and modulating immune reactivity. *Biomaterials* **156**, 16–27 (2018).

45. Zhu, Y. Z. *et al.* Extracellular Vesicles Derived from Human Adipose-Derived Stem Cell Prevent the Formation of Hypertrophic Scar in a Rabbit Model. *Ann Plast Surg* **84**, 602–607 (2020).

46. LeSavage, B. L., Suhar, R. A., Broguiere, N., Lutolf, M. P. & Heilshorn, S. C. Next-generation cancer organoids. *Nature Materials* vol. 21 143–159 Preprint at https://doi.org/10.1038/s41563-021-01057-5 (2022).

47. Jensen, C. & Teng, Y. Is It Time to Start Transitioning From 2D to 3D Cell Culture? *Frontiers in Molecular Biosciences* vol. 7 Preprint at https://doi.org/10.3389/fmolb.2020.00033 (2020).

48. Wilding, J. L. & Bodmer, W. F. Cancer cell lines for drug discovery and development. *Cancer Research* vol. 74 2377–2384 Preprint at https://doi.org/10.1158/0008-5472.CAN-13-2971 (2014).

49. Duval, K. *et al.* Modeling physiological events in 2D vs. 3D cell culture. *Physiology* vol. 32 266–277 Preprint at https://doi.org/10.1152/physiol.00036.2016 (2017).

50. Gillet, J. P., Varma, S. & Gottesman, M. M. The clinical relevance of cancer cell lines. *Journal of the National Cancer Institute* vol. 105 452–458 Preprint at https://doi.org/10.1093/jnci/djt007 (2013).

51. Katt, M. E., Placone, A. L., Wong, A. D., Xu, Z. S. & Searson, P. C. In vitro tumor models: Advantages, disadvantages, variables, and selecting the right platform. *Frontiers in Bioengineering and Biotechnology* vol. 4 Preprint at https://doi.org/10.3389/fbioe.2016.00012 (2016).

52. Mcmillin, D. W., Negri, J. M. & Mitsiades, C. S. The role of tumour-stromal interactions in modifying drug response: Challenges and opportunities. *Nature Reviews Drug Discovery* vol. 12 217–228 Preprint at https://doi.org/10.1038/nrd3870 (2013).

53. Melissaridou, S. *et al.* The effect of 2D and 3D cell cultures on treatment response, EMT profile and stem cell features in head and neck cancer. *Cancer Cell Int* **19**, (2019).

54. Stock, K. *et al.* Capturing tumor complexity in vitro: Comparative analysis of 2D and 3D tumor models for drug discovery. *Sci Rep* **6**, (2016).

55. Yuki, K., Cheng, N., Nakano, M. & Kuo, C. J. Organoid Models of Tumor Immunology. *Trends in Immunology* vol. 41 652–664 Preprint at https://doi.org/10.1016/j.it.2020.06.010 (2020).

56. Kersten, K., de Visser, K. E., van Miltenburg, M. H. & Jonkers, J. Genetically engineered mouse models in oncology research and cancer medicine. *EMBO Mol Med* **9**, 137–153 (2017).

57. Lai, Y. *et al.* Current status and perspectives of patient-derived xenograft models in cancer research. *Journal of Hematology and Oncology* vol. 10 Preprint at https://doi.org/10.1186/s13045-017-0470-7 (2017).

58. De Angelis, M. L. *et al.* An Orthotopic Patient-Derived Xenograft (PDX) Model Allows the Analysis of Metastasis-Associated Features in Colorectal Cancer. *Front Oncol* **12**, (2022).

59. Derose, Y. S. *et al.* Tumor grafts derived from women with breast cancer authentically reflect tumor pathology, growth, metastasis and disease outcomes. *Nat Med* **17**, 1514–1520 (2011).

60. Gao, H. *et al.* High-throughput screening using patient-derived tumor xenografts to predict clinical trial drug response. *Nat Med* **21**, 1318–1325 (2015).

61. Hoffman, R. M. Patient-derived orthotopic xenografts: Better mimic of metastasis than subcutaneous xenografts. *Nature Reviews Cancer* vol. 15 451–452 Preprint at https://doi.org/10.1038/nrc3972 (2015).

62. Choi, Y. *et al.* Studying cancer immunotherapy using patient-derived xenografts (PDXs) in humanized mice. *Experimental and Molecular Medicine* vol. 50 Preprint at https://doi.org/10.1038/s12276-018-0115-0 (2018).

63. Yada, E., Wada, S., Yoshida, S. & Sasada, T. Use of patient-derived xenograft mouse models in cancer research and treatment. *Future Science OA* vol. 4 Preprint at https://doi.org/10.4155/fsoa-2017-0136 (2018).

64. Olson, B., Li, Y., Lin, Y., Liu, E. T. & Patnaik, A. Mouse models for cancer immunotherapy research. *Cancer Discovery* vol. 8 1358–1365 Preprint at https://doi.org/10.1158/2159-8290.CD-18-0044 (2018).

65. Byrne, A. T. *et al.* Interrogating open issues in cancer precision medicine with patient-derived xenografts. *Nature Reviews Cancer* vol. 17 254–268 Preprint at https://doi.org/10.1038/nrc.2016.140 (2017).

66. Bissell, M. J. Goodbye flat biology - time for the 3rd and the 4th dimensions. *Journal of Cell Science* vol. 130 3–5 Preprint at https://doi.org/10.1242/jcs.200550 (2017).

67. Rodrigues, J., Heinrich, M. A., Teixeira, L. M. & Prakash, J. 3D In Vitro Model (R)evolution: Unveiling Tumor–Stroma Interactions. *Trends in Cancer* vol. 7 249–264 Preprint at https://doi.org/10.1016/j.trecan.2020.10.009 (2021).

68. Hirschhaeuser, F. *et al.* Multicellular tumor spheroids: An underestimated tool is catching up again. *J Biotechnol* **148**, 3–15 (2010).

69. Sant, S. & Johnston, P. A. The production of 3D tumor spheroids for cancer drug discovery. *Drug Discovery Today: Technologies* vol. 23 27–36 Preprint at https://doi.org/10.1016/j.ddtec.2017.03.002 (2017).

70. LaBarbera, D. V., Reid, B. G. & Yoo, B. H. The multicellular tumor spheroid model for high-throughput cancer drug discovery. *Expert Opinion on Drug Discovery* vol. 7 819–830 Preprint at https://doi.org/10.1517/17460441.2012.708334 (2012).

71. Abbott, R. D. & Kaplan, D. L. Strategies for improving the physiological relevance of human engineered tissues. *Trends in Biotechnology* vol. 33 401–407 Preprint at https://doi.org/10.1016/j.tibtech.2015.04.003 (2015).

72. Sontheimer-Phelps, A., Hassell, B. A. & Ingber, D. E. Modelling cancer in microfluidic human organs-on-chips. *Nature Reviews Cancer* vol. 19 65–81 Preprint at https://doi.org/10.1038/s41568-018-0104-6 (2019).

73. Clevers, H. Modeling Development and Disease with Organoids. *Cell* vol. 165 1586–1597 Preprint at https://doi.org/10.1016/j.cell.2016.05.082 (2016).

74. Drost, J. & Clevers, H. Organoids in cancer research. *Nature Reviews Cancer* vol. 18 407–418 Preprint at https://doi.org/10.1038/s41568-018-0007-6 (2018).

75. Lancaster, M. A. & Knoblich, J. A. Organogenesisin a dish: Modeling development and disease using organoid technologies. *Science* vol. 345 Preprint at https://doi.org/10.1126/science.1247125 (2014).

76. Crespo, M. *et al.* Colonic organoids derived from human induced pluripotent stem cells for modeling colorectal cancer and drug testing. *Nat Med* **23**, 878–884 (2017).

77. Drost, J. *et al.* Use of CRISPR-modified human stem cell organoids to study the origin of mutational signatures in cancer. *Science (1979)* **358**, 234–238 (2017).

78. Van De Wetering, M. *et al.* Prospective derivation of a living organoid biobank of colorectal cancer patients. *Cell* **161**, 933–945 (2015).

79. Gao, D. *et al.* Organoid cultures derived from patients with advanced prostate cancer. *Cell* **159**, 176–187 (2014).

80. Weeber, F. *et al.* Preserved genetic diversity in organoids cultured from biopsies of human colorectal cancer metastases. *Proc Natl Acad Sci U S A* **112**, 13308–13311 (2015).

81. Bar-Ephraim, Y. E., Kretzschmar, K. & Clevers, H. Organoids in immunological research. *Nature Reviews Immunology* vol. 20 279–293 Preprint at https://doi.org/10.1038/s41577-019-0248-y (2020).

82. Manduca, N., Maccafeo, E., De Maria, R., Sistigu, A. & Musella, M. 3D cancer models: One step closer to in vitro human studies. *Frontiers in Immunology* vol. 14 Preprint at https://doi.org/10.3389/fimmu.2023.1175503 (2023).

83. Urabe, F. *et al.* Extracellular vesicles as biomarkers and therapeutic targets for cancer. *Extracellular Vesicles in Cell Physiology Am J Physiol Cell Physiol* **318**, 29–39 (2020).

84. Kosaka, N. *et al.* Exploiting the message from cancer: the diagnostic value of extracellular vesicles for clinical applications. *Experimental and Molecular Medicine* vol. 51 Preprint at https://doi.org/10.1038/s12276-019-0219-1 (2019).

85. Weston, W. W., Ganey, T. & Temple, H. T. The Relationship between Exosomes and Cancer: Implications for Diagnostics and Therapeutics. *BioDrugs* vol. 33 137–158 Preprint at https://doi.org/10.1007/s40259-019-00338-5 (2019).

86. Urabe, F., Kosaka, N., Kimura, T., Egawa, S. & Ochiya, T. Extracellular vesicles: Toward a clinical application in urological cancer treatment. *International Journal of Urology* vol. 25 533–543 Preprint at https://doi.org/10.1111/iju.13594 (2018).

87. Crescitelli, R., Lässer, C. & Lötvall, J. Isolation and characterization of extracellular vesicle subpopulations from tissues. *Nat Protoc* **16**, 1548–1580 (2021).

88. Logozzi, M. *et al.* Microenvironmental pH and exosome levels interplay in human cancer cell lines of different histotypes. *Cancers (Basel)* **10**, (2018).

89. Nogués, L., Benito-Martin, A., Hergueta-Redondo, M. & Peinado, H. The influence of tumour-derived extracellular vesicles on local and distal metastatic dissemination. *Molecular Aspects of Medicine* vol. 60 15–26 Preprint at https://doi.org/10.1016/j.mam.2017.11.012 (2018).

90. Rahbarghazi, R. *et al.* Tumor-derived extracellular vesicles: Reliable tools for Cancer diagnosis and clinical applications. *Cell Communication and Signaling* vol. 17 Preprint at https://doi.org/10.1186/s12964-019-0390-y (2019).

91. Chang, L. C., Chiu, H. M., Wu, M. S. & Shen, T. L. The Role of Small Extracellular Vesicles in the Progression of Colorectal Cancer and Its Clinical Applications. *International Journal of Molecular Sciences* vol. 23 Preprint at https://doi.org/10.3390/ijms23031379 (2022).

92. D'angelo, E. *et al.* Patient-derived scaffolds of colorectal cancer metastases as an organotypic 3D model of the liver metastatic microenvironment. *Cancers (Basel)* **12**, (2020).

93. Giebel, B., Kordelas, L. & Börger, V. Clinical potential of mesenchymal stem/stromal cell-derived extracellular vesicles. *Stem Cell Investigation* vol. 4 Preprint at https://doi.org/10.21037/sci.2017.09.06 (2017).

94. Peichev, M. *et al.* Expression of VEGFR-2 and AC133 by circulating human CD34+ cells identifies a population of functional endothelial precursors. *Blood* **95**, 952–958 (2000).

95. Bordanaba-Florit, G., Madarieta, I., Olalde, B., Falcón-Pérez, J. M. & Royo, F. 3D cell cultures as prospective models to study extracellular vesicles in cancer. *Cancers (Basel)* **13**, 1–17 (2021).

96. Logozzi, M. *et al.* Microenvironmental pH and exosome levels interplay in human cancer cell lines of different histotypes. *Cancers (Basel)* **10**, (2018).

97. Hoshino, A. *et al.* Extracellular Vesicle and Particle Biomarkers Define Multiple Human Cancers. *Cell* **182**, 1044-1061.e18 (2020).

98. Lunavat, T. R. *et al.* BRAFV600 inhibition alters the microRNA cargo in the vesicular secretome of malignant melanoma cells. *Proc Natl Acad Sci U S A* **114**, E5930–E5939 (2017).

99. Jingushi, K. *et al.* Extracellular vesicles isolated from human renal cell carcinoma tissues disrupt vascular endothelial cell morphology via azurocidin. *Int J Cancer* **142**, 607–617 (2018).

100. Martins Castanheira, N., Spanhofer, A. K., Wiener, S., Bobe, S. & Schillers, H. Uptake of platelets by cancer cells and recycling of the platelet protein CD42a. *Journal of Thrombosis and Haemostasis* **20**, 170–181 (2022).

101. Gao, Q. *et al.* CD142 plays an important role in the mobility of colorectal cancer cells. *Bioscience, Biotechnology and Biochemistry* vol. 84 1856–1860 Preprint at https://doi.org/10.1080/09168451.2020.1772039 (2020).

102. Palacios-Acedo, A. L. *et al.* Platelets, Thrombo-Inflammation, and Cancer: Collaborating With the Enemy. *Frontiers in immunology* vol. 10 1805 Preprint at https://doi.org/10.3389/fimmu.2019.01805 (2019).

103. Chiesa, M. Della *et al.* NK Cell-Based Immunotherapy in Colorectal Cancer. *Vaccines* vol. 10 Preprint at https://doi.org/10.3390/vaccines10071033 (2022).

104. Wylie, B., Macri, C., Mintern, J. D. & Waithman, J. Dendritic cells and cancer: From biology to therapeutic intervention. *Cancers (Basel)* **11**, (2019).

105. Dunne, M. R. *et al.* Characterising the prognostic potential of HLA-DR during colorectal cancer development. *Cancer Immunology, Immunotherapy* **69**, 1577–1588 (2020).

106. Han, S. H. *et al.* Expression of HLA class I is associated with immune cell infiltration and patient outcome in breast cancer. *Sci Rep* **12**, (2022).

107. Liu, D. *et al. Oncotarget 40704 www.impactjournals.com/oncotarget Reduced CD146 expression promotes tumorigenesis and cancer stemness in colorectal cancer through activating Wnt/β-catenin signaling*. *Oncotarget* vol. 7 www.impactjournals.com/oncotarget/.

108. Zhou, H. *et al.* Liquid biopsy at the frontier of detection, prognosis and progression monitoring in colorectal cancer. *Molecular Cancer* vol. 21 Preprint at https://doi.org/10.1186/s12943-022-01556-2 (2022).

109. Galon, J. *et al.* Type, Density, and Location of Immune Cells Within Human Colorectal Tumors Predict Clinical Outcome. *Science (1979)* **313**, 1960–1964 (2006).

110. Angell, H. K., Bruni, D., Carl Barrett, J., Herbst, R. & Galon, J. The immunoscore: Colon cancer and beyond a C. *Clinical Cancer Research* **26**, 332–339 (2020).

111. Mlecnik, B. *et al.* Histopathologic-based prognostic factors of colorectal cancers are associated with the state of the local immune reaction. *Journal of Clinical Oncology* **29**, 610–618 (2011).

112. Kotsafti, A. *et al.* Immune surveillance activation after neoadjuvant therapy for esophageal adenocarcinoma and complete response. *Oncoimmunology* **9**, (2020).

113. Bergsland, C. H. *et al.* Spatial analysis and CD25-expression identify regulatory T cells as predictors of a poor prognosis in colorectal cancer. *Modern Pathology* **35**, 1236–1246 (2022).

114. Peng, Y. *et al.* CD25: A potential tumor therapeutic target. *Int J Cancer* **152**, 1290–1303 (2023).

115. Liyanage, U. K. *et al.* Prevalence of regulatory T cells is increased in peripheral blood and tumor microenvironment of patients with pancreas or breast adenocarcinoma. *J Immunol* **169**, 2756–2761 (2002).

116. Miller, A. M. *et al.* CD4+CD25high T cells are enriched in the tumor and peripheral blood of prostate cancer patients. *J Immunol* **177**, 7398–7405 (2006).

117. Spees, J. L., Lee, R. H. & Gregory, C. A. Mechanisms of mesenchymal stem/stromal cell function. *Stem Cell Research and Therapy* vol. 7 Preprint at https://doi.org/10.1186/s13287-016-0363-7 (2016).

118. Weng, Z. *et al.* Therapeutic roles of mesenchymal stem cell-derived extracellular vesicles in cancer. *Journal of Hematology and Oncology* vol. 14 Preprint at https://doi.org/10.1186/s13045-021-01141-y (2021).

119. Nawaz, M. *et al.* Review extracellular vesicles and matrix remodeling enzymes: The emerging roles in extracellular matrix remodeling, progression of diseases and tissue repair. *Cells* **7**, (2018).

120. Sanderson, R. D., Bandari, S. K. & Vlodavsky, I. Proteases and glycosidases on the surface of exosomes: Newly discovered mechanisms for extracellular remodeling. *Matrix Biology* vols 75–76 160–169 Preprint at https://doi.org/10.1016/j.matbio.2017.10.007 (2019).

121. Rilla, K. *et al.* Extracellular vesicles are integral and functional components of the extracellular matrix. *Matrix Biology* **75–76**, 201–219 (2019).

122. Lee, Y., El Andaloussi, S. & Wood, M. J. A. Exosomes and microvesicles: Extracellular vesicles for genetic information transfer and gene therapy. *Hum Mol Genet* **21**, (2012).

123. El Andaloussi, S., Mäger, I., Breakefield, X. O. & Wood, M. J. A. Extracellular vesicles: Biology and emerging therapeutic opportunities. *Nature Reviews Drug Discovery* vol. 12 347–357 Preprint at https://doi.org/10.1038/nrd3978 (2013).

124. Pio, R., Corrales, L. & Lambris, J. D. The role of complement in tumor growth. in *Advances in Experimental Medicine and Biology* vol. 772 229–262 (Springer New York LLC, 2014).

125. Nauta, A. J. *et al.* Biochemical and functional characterization of the interaction between pentraxin 3 and C1q. *European Journal of Immunology* vol. 33 465–473 Preprint at https://doi.org/10.1002/immu.200310022 (2003).

126. Roumenina, L. T., Daugan, M. V., Petitprez, F., Sautès-Fridman, C. & Fridman, W. H. Context-dependent roles of complement in cancer. *Nature Reviews Cancer* vol. 19 698–715 Preprint at https://doi.org/10.1038/s41568-019-0210-0 (2019).

127. Bonavita, E. *et al.* PTX3 is an extrinsic oncosuppressor regulating complement-dependent inflammation in cancer. *Cell* **160**, 700–714 (2015).

128. Luk, S. C. W. *et al. In Vivo and In Vitro Association of 14-3-3 Epsilon Isoform With Calmodulin: Implication for Signal Transduction and Cell Proliferation*. *J. Cell. Biochem* vol. 73 (1999).

129. Jiang, Y. *et al.* Prosaposin promotes the proliferation and tumorigenesis of glioma through toll-like receptor 4 (TLR4)-mediated NF-κB signaling pathway. *EBioMedicine* **37**, 78–90 (2018).

130. Biaoxue, R., Xiguang, C., Hua, L. & Shuanying, Y. Stathmin-dependent molecular targeting therapy for malignant tumor: The latest 5 years' discoveries and developments. *Journal of Translational Medicine* vol. 14 Preprint at https://doi.org/10.1186/s12967-016-1000-z (2016).

131. Li, L. *et al.* Human mesenchymal stem cells play a dual role on tumor cell growth in vitro and in vivo. *J Cell Physiol* **226**, 1860–1867 (2011).

132. Bruno, S. *et al.* Microvesicles derived from human bone marrow mesenchymal stem cells inhibit tumor growth. *Stem Cells Dev* **22**, 758–771 (2013).

133. Sage, E. H. & Bornstein, P. Extracellular, proteins that modulate cell-matrix interactions. Sparc, tenascin, and thrombospondin. *Journal of Biological Chemistry* vol. 266 14831–14834 Preprint at https://doi.org/10.1016/s0021-9258(18)98545-5 (1991).

134. Tai, I. T. & Tang, M. J. SPARC in cancer biology: Its role in cancer progression and potential for therapy. *Drug Resistance Updates* **11**, 231–246 (2008).

135. Zhu, A. *et al. Oncotarget 76628 www.impactjournals.com/oncotarget SPARC overexpression in primary tumors correlates with disease recurrence and overall survival in patients with triple negative breast cancer*. *Oncotarget* vol. 7 www.impactjournals.com/oncotarget/.

136. Funk, S. E. & Sage, E. H. *The Ca2+-binding glycoprotein SPARC modulates cell cycle progression in bovine aortic endothelial cells (extracellular matrix)*. *Proc. Nati. Acad. Sci. USA* vol. 88 (1991).

137. Zheng, P., Wang, Q., Teng, J. & Chen, J. Calumenin and fibulin-1 on tumor metastasis: Implications for pharmacology. *Pharmacological Research* vol. 99 11–15 Preprint at https://doi.org/10.1016/j.phrs.2015.05.001 (2015).

138. Klepinin, A. *et al.* Adenylate Kinase and Metabolic Signaling in Cancer Cells. *Frontiers in Oncology* vol. 10 Preprint at https://doi.org/10.3389/fonc.2020.00660 (2020).

139. Kim, H. *et al.* AK2 is an AMP-sensing negative regulator of BRAF in tumorigenesis. *Cell Death Dis* **13**, (2022).

140. Cai, F. *et al.* AK2 Promotes the Migration and Invasion of Lung Adenocarcinoma by Activating TGF-β/Smad Pathway In vitro and In vivo. *Front Pharmacol* **12**, (2021).

141. Hansel, D. E. *et al. Met Proto-Oncogene and Insulin-Like Growth Factor Binding Protein 3 Overexpression Correlates with Metastatic Ability in Well-Differentiated Pancreatic Endocrine Neoplasms*. http://www.ncbi.nlm.nih.gov/PubMed.